Cancer tissue of origin constrains the growth and metabolism of metastases

Sharanya Sivanand[1,2], Yetis Gultekin[1,2,19], Peter S. Winter[1,3,4,5,19],
Sidney Y. Vermeulen[1,2,19], Konstantine M. Tchourine [6,19], Keene L. Abbott [1,2,4],
Laura V. Danai[1,2,7], Florian Gourgue [1,2], Brian T. Do [1,5], Kayla Crowder[8],
Tenzin Kunchok [8], Allison N. Lau [1,2], Alicia M. Darnell[1,2],
Alexandria Jefferson[1,2,8], Satoru Morita[9], Dan G. Duda [9],
Andrew J. Aguirre [3,4,10], Brian M. Wolpin [3], Nicole Henning[1,11],
Virginia Spanoudaki[1,11], Laura Maiorino [1], Darrell J. Irvine [1,12,13,14],
Omer H. Yilmaz [1,2,4,15], Caroline A. Lewis [8,16], Dennis Vitkup[6,17],
Alex K. Shalek [1,4,5,14,18] & Matthew G. Vander Heiden [1,2,3,4] ✉

Metastases arise from subsets of cancer cells that disseminate from the primary tumour[1,2]. The ability of cancer cells to thrive in a new tissue site is influenced by genetic and epigenetic changes that are important for disease initiation and progression, but these factors alone do not predict if and where cancers metastasize[3,4]. Specific cancer types metastasize to consistent subsets of tissues, suggesting that primary tumour-associated factors influence where cancers can grow. We find primary and metastatic pancreatic tumours have metabolic similarities and that the tumour-initiating capacity and proliferation of both primary-derived and metastasis-derived cells is favoured in the primary site relative to the metastatic site. Moreover, propagating cells as tumours in the lung or the liver does not enhance their relative ability to form large tumours in those sites, change their preference to grow in the primary site, nor stably alter aspects of their metabolism relative to primary tumours. Primary liver and lung cancer cells also exhibit a preference to grow in their primary site relative to metastatic sites. These data suggest cancer tissue of origin influences both primary and metastatic tumour metabolism and may impact where cancer cells can metastasize.

Metabolism is influenced by available nutrients, and this can determine a preference for cancers to grow in primary and metastatic sites[5–7]. The nutrients available to cancer cells and cancer metabolic phenotypes are both influenced by cancer tissue of origin and tumour location[8–12], yet cancer cells also exhibit metabolic plasticity to enable proliferation in metastatic sites[13–17]. However, tumour metabolic gene expression better resembles the tissue of origin for a cancer than it does tumours arising in other tissues[18,19], and differences in tissue nutrient availability may also constrain the tissue-of-origin-shaped metabolism of cancer cells to limit sites of metastatic colonization[10,18–20]. This model would predict some metabolic similarities are retained between the primary and metastatic tumours, and that aspects of metastatic tumour metabolism are influenced by the tissue of origin, a possibility that has not been tested. This led us to investigate how well primary-derived and metastasis-derived cancer cells grow in different tissues, and how metabolism of primary and metastatic tumours relates to their preferences to grow in different tissue sites.

Pancreatic ductal adenocarcinoma (PDAC) has a high incidence of metastasis. The genetically engineered *LSL-Kras[G12D/+]*; *Trp53[R172H/+]*; *Pdx1-Cre* (KPC) mouse PDAC model develops liver, and occasionally

lung, metastases, similarly to humans[21]. To study primary and metastatic PDAC, cancer cells were isolated from primary tumours and matched liver or lung metastases from the KPC model. These cells express mutant Kras and proliferate at similar rates in standard culture conditions (Extended Data Fig. 1a–d). To confirm an increased ability of metastasis-derived PDAC cells to colonize the organ to which it had metastasized[17,22], primary-derived and liver metastasis-derived cells were engineered to express either mCherry or GFP, such that equal numbers of cells expressing different fluorescent proteins could be mixed and implanted into the pancreas, liver or flank (subcutaneous) in syngeneic C57BL/6J mice (Extended Data Fig. 1e). A fixed number of cells formed tumours of similar size in the pancreas when injected individually, or co-injected as a mixed population, despite expressing different fluorescent proteins (Extended Data Fig. 1f,g). When a mixed population of primary-derived and liver metastasis-derived cells were implanted in the pancreas, the resulting tumours were enriched for primary tumour-derived cells when analysed by either flow cytometry or immunohistochemistry, regardless of the fluorophore expressed (Extended Data Fig. 1h–j), even though mCherry is more immunogenic than GFP[23]. As expected, when implanted in the liver, liver metastases-derived cells were more abundant regardless of mCherry or GFP expression, even though primary tumour-derived cells also contributed (Extended Data Fig. 1k–m). When a mixed population of primary-derived and liver metastasis-derived cells were implanted in the flank, the resulting tumour was derived primarily from one of the two cell populations, and this was not determined by fluorescent protein expression (Extended Data Fig. 1n,o). These data are consistent with tumours at either the primary or the metastatic site being derived from a subset of cancer cells and confirm the cells exhibit known phenotypes associated with metastasis-derived cells, including an increased ability to metastasize to the site from which they were derived[24].

The flank is a site not previously experienced by primary or liver metastatic PDAC cells. Since tumours in this site were derived predominantly from subsets of cells (Extended Data Fig. 1n,o), stochastic processes related to metastasis being a rare event[2] may influence which cells contribute to the tumour[1,25,26]. To test this possibility further, we labelled primary pancreatic cancer cells with either mCherry or GFP, mixed them in equal proportions (Fig. 1a), and implanted the mixed population into the pancreas, liver or flank. Despite the different labelled cancer cells being derived from the same cell population, in most cases either mCherry-expressing or GFP-expressing cells were found to be dominant in tumours that formed regardless of site, and this phenotype was not affected by the fluorescent protein expressed (Fig. 1b–d). These data are not only consistent with observations of clonal dominance in both primary and metastatic PDAC[27], but also suggest subclones from the primary tumour in metastases can reflect, at least in part, stochastic events that result in cell subsets contributing to tumours in different locations.

Several studies report that specific nutrient availability can determine whether cancer cells grow in a metastatic site[28]; however, those studies have focused on how metabolism of specific tissue metastases differs from the primary tumour, and a comprehensive analysis of both the metabolic similarities and differences for primary and metastatic tumours growing in different sites is lacking. To determine whether accessing a tissue nutrient environment with sufficient similarity to the primary site is important to support the metabolism of metastatic cancer cells, we implanted primary-derived or liver metastasis-derived PDAC cells into the pancreas or liver to form tumours in mice. This approach was needed to generate large enough tumours for analysis of isotopically labelled glucose fate in tumours growing in each site[29]. Tumour-bearing mice were analysed after a 6-h ^{13}C-labelled glucose infusion, a time where metabolite labelling approaches steady state allowing comparison of glucose fate between tissues[29]. Similar ^{13}C-labelled glucose enrichment was observed in plasma of mice infused with labelled glucose bearing either pancreatic tumours or liver

metastatic tumours (Extended Data Fig. 2a), and minimal differences in glucose fate were observed when comparing metabolite labelling in tumours growing in the pancreas or liver (Fig. 1e–l). To extend these findings to a second PDAC mouse model, we implanted cancer cells isolated from the *LSL-Kras$^{G12D/+}$; Trp53$^{-/-}$; Pdx1-Cre* (KP$^{-/-}$C) model[30,31] into the pancreas, liver or flank and compared [U-^{13}C]glucose in these tumours to the normal pancreas and liver. While a different labelling pattern was observed for some metabolites when comparing tumours and normal tissues, minimal metabolite labelling differences were observed in pancreatic tumours growing in different tissues (Extended Data Fig. 2b–i). We also found minimal differences in metabolite labelling from infused [U-^{13}C]glutamine in KP$^{-/-}$C PDAC-derived pancreas or liver tumours (Extended Data Fig. 2j–o). Together, these data argue that in the PDAC models studied, there are many similarities in how glucose and glutamine are metabolized in primary and metastatic tumours even though glucose metabolism in the tumours differs from that observed in normal pancreas and liver.

We next compared metabolite levels measured in primary pancreatic tumours and matched liver metastases with those measured in normal pancreas and liver from age-matched mice (Supplementary Table 1). Unsupervised clustering suggested that metabolite levels in normal liver are most distinct from the other samples (Fig. 1m). Moreover, this revealed less separation between primary tumours, liver metastases, and the normal pancreas relative to the normal liver when the same data were analysed using two different approaches (Fig. 1m,n). Of note, although variability across samples is observed, evidence for consistent changes in metabolites that distinguish primary and liver metastatic tumours from KPC mice is lacking (Extended Data Fig. 2p). Taken together with the data assessing glucose and glutamine fate, these data suggest that aspects of metabolism are shared between the primary tumour and liver metastasis, and that the metabolic phenotype of a pancreatic cancer liver metastasis more closely resembles the primary tumour and normal tissue of origin than it does the metastatic tissue.

We next examined metabolite levels in cultured PDAC cells and found metabolite levels were similar across different independently derived paired primary and liver metastatic cells such that clustering based on metabolites did not uniformly segregate primary cells from liver metastatic cells (Extended Data Fig. 3a and Supplementary Table 2). We also assessed [U-^{13}C]glucose fate in these cells to examine whether nutrient utilization differs in culture. Although some differences in glucose fate were observed across select primary-derived and liver metastasis-derived cells, these differences were not consistent across multiple paired primary and liver metastatic lines from independent mice (Extended Data Fig. 3b–j). Together, these data argue that any major metabolic differences that exist between primary and liver metastatic PDAC cells are not maintained in standard culture, and thus are not determined by stable genetic or epigenetic control of metabolism. However, these data should not be interpreted to say there are no metabolic differences between primary pancreatic tumours and liver metastases.

If the need to access a tissue environment with enough similarity to the primary tissue site is a barrier to metastasis, we reasoned that this may result in metastatic cancer cells retaining a preference to grow in the primary site. For instance, if a specific nutrient environment is needed to support the growth of either primary or metastatic tumours, this environment would be better represented in the primary tissue and result in differences in the rate of tumour growth in different sites. Prior studies of metastasis have focused on how metabolism impacts whether cancer cells can exit the primary tumour, survive in circulation or find and grow in a particular site[28,32]. However, to our knowledge, the preferential ability of cancer cells derived from primary and metastatic tumours to expand in different tissues after colonization has been largely unexplored. To examine this, we implanted cells derived from either primary KPC tumours or matched
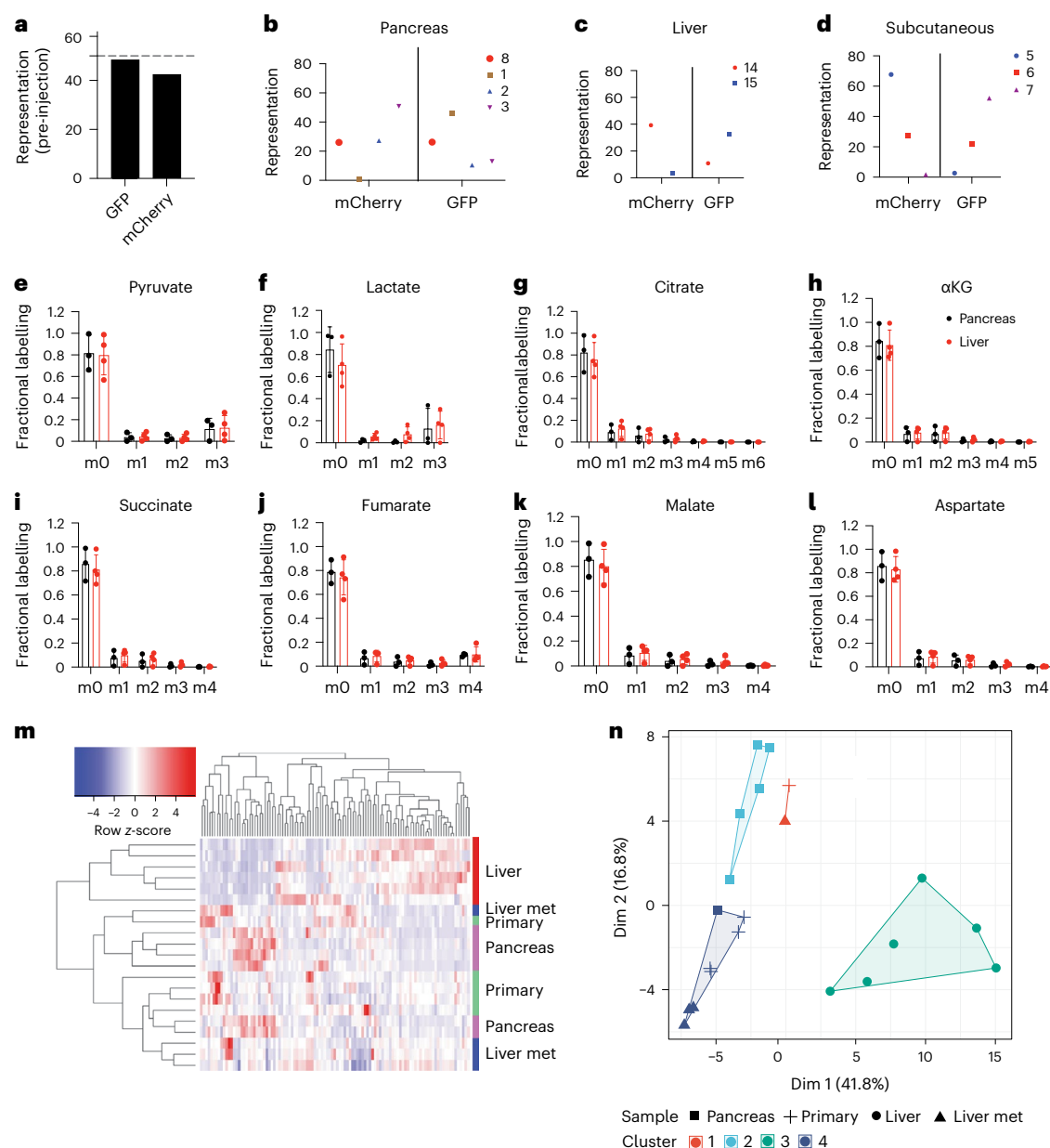
Fig. 1 | Primary and metastatic pancreatic tumours exhibit some similar metabolic phenotypes. a, The same cancer cells isolated from a primary pancreatic tumour arising in a KPC mouse were engineered to express either mCherry or GFP and combined in equal numbers before implantation into different tissue sites in mice. Flow cytometry confirmed that an approximately equal representation of each labelled cancer cell population is present in the mixed population. **b–d**, Representation of mCherry- and GFP-labelled cells in tumours derived from injection of the mixed population shown in **a** into the pancreas (n = 4) (**b**), liver (n = 2) (**c**) or subcutaneous space (n = 3) (**d**). **e–l**, Paired pancreatic cancer cells derived from primary tumours or liver metastases arising in the KPC mouse model were implanted into the pancreas or liver, respectively, and the resulting tumour-bearing mice were infused for 6 h with [U-^{13}C]glucose at 0.4 mg min^{-1} to assess glucose fate in tumours growing in each site. Fractional labelling of the indicated metabolites as determined by gas chromatography–mass spectrometry is shown. Data are from n = 3–4 mice per group; mean ± s.d. **m,n**, Relative metabolite levels in autochthonous paired primary pancreatic cancer and liver metastases arising in KPC mice were assessed by liquid chromatography–mass spectrometry; tumours were harvested in the mornings at the same time of the day. Metabolite levels were also measured for normal pancreas and liver tissue from age-matched, non-tumour-bearing control mice. The metabolite data for each sample were clustered in two different ways: unsupervised clustering represented as k-means unsupervised clustering (**m**) or as a heat map (**n**); n = 6 mice were used for the normal tissue analysis and n = 4 mice were used for the paired primary tumour and metastasis analysis.

liver metastases into the pancreas, liver or flank (Fig. 2a). In all cases, the cells lacked any fluorophore expression, and the same number of cells were implanted in each site before analysis of tumour size after 4 weeks. We assessed tumour weight where possible, or if too small to accurately weigh, we assessed the weight of the tumour-bearing organ as well as the weight of the corresponding normal tissue from age-matched mice. We found that cancer cells from both primary and liver metastatic tumours were able to form tumours at all sites,

but observed much larger tumours forming in the pancreas regardless of whether the cancer cells were derived from primary tumours or liver metastases (Fig. 2b and Extended Data Fig. 4a,b). Interestingly, cancer cells formed tumours that grew to a similar size in each organ site regardless of whether the cells were derived from a primary or a liver metastatic lesion. Tumours in each site were also histologically similar, with tumour grade similar to naturally arising primary and liver metastatic tumours in KPC mice (Extended Data Fig. 4c,d,f and

Supplementary Table 1). Cell proliferation as determined by either Ki67 or BrdU staining in tumours formed from primary-derived or liver metastasis-derived cells in the pancreas was similar, as was assessment of proliferation when the cells formed tumours in the liver (Fig. 2c,e and Extended Data Fig. 5a,d). Cleaved caspase-3 staining was assessed as a cell death marker, and tumours formed from primary-derived or liver metastasis-derived cells in the pancreas had comparable staining, as did tumours formed from primary-derived or liver metastasis-derived cells in the liver (Fig. 2f and Extended Data Fig. 5e,f). Of note, regardless of whether the tumour was derived from primary-derived or liver metastasis-derived cells, both Ki67 and BrdU staining trended lower, and cleaved caspase-3 staining trended higher in tumours growing in the liver compared to the pancreas, a finding consistent with larger tumours forming in the pancreas. We repeated the transplantation experiments with independently derived tdTomato-expressing paired primary and liver metastasis lines and found a similar preference to form larger tumours in the pancreas (Extended Data Fig. 6a). These data argue the pancreas better supports the growth of pancreatic cancer cells as tumours, even if those cancer cells are derived from liver metastasis.

The fact that immunogenic tdTomato fluorophore expression did not affect the preference for both primary-derived and liver metastasis-derived cells to grow in the pancreas argues against a tissue-specific difference in adaptive immunity explaining this phenotype; however, to further test this possibility, we implanted the same number of paired primary tumour or liver metastasis-derived PDAC cells into the pancreas or liver of nude mice that lack T cells, and we again observed after a fixed time that both primary tumour-derived and liver metastasis-derived PDAC cells formed larger tumours in the pancreas (Fig. 2h and Extended Data Fig. 6b). Weight loss was noted in some nude mice following tumour implantation that was not observed when cells were implanted into syngeneic hosts. To control for this, we normalized tumour size data to body weight, and still observed a preference for both primary tumour-derived and liver metastasis-derived cells to grow in the pancreas compared to the liver (Extended Data Fig. 6c,d). These data argue that a preference for PDAC cells to grow in the pancreas relative to the liver cannot be explained by tissue-specific differences in T cell-mediated immune responses.

To examine tumour-initiating capacity in different tissues, we implanted different numbers of either primary-derived or liver metastasis-derived PDAC cells into the pancreas or liver and determined the minimal number of cells required to form tumours in each site. Both primary-derived and liver metastasis-derived cells have similar tumour-initiating capacity at each site; however, fewer cells can initiate tumours in the pancreas compared to the liver, regardless of whether the cells are from a PDAC primary or liver metastasis tumour (Fig. 2i,j). These data further support a preference for PDAC cells to grow in the primary site even if derived from a liver metastasis.

To assess whether PDAC lung metastatic cells also retain a preference to grow in the pancreas, we performed similar experiments using independently derived cells that lack fluorophore expression from matched primary, liver and lung metastases arising in KPC mice (Extended Data Fig. 4e). Cells derived from either liver metastases or lung metastases form tumours in both the liver and lung; however, the largest tumours developed in the pancreas and the smallest tumours developed in the flank (Fig. 2k and Extended Data Fig. 7a–f). We confirmed using cells from an independently derived liver metastasis that liver metastatic PDAC does not have an enhanced ability to grow in the lung (Extended Data Fig. 7g–i). The tumours forming in the lung were histologically similar regardless of whether they were derived from a primary tumour or metastasis (Extended Data

Fig. 2 | Pancreatic cancer cells derived from both the primary tumour and from metastatic sites generate tumours that grow fastest in the pancreas.
a, Schematic depicting transplantation experiments to quantitatively assess pancreatic cancer cell proliferation in different tissue sites. Created with BioRender.com. **b**, Equal numbers of cancer cells isolated from primary pancreatic tumours or paired liver metastases arising in the KPC mouse model were implanted into the pancreas, liver or subcutaneous space, and resulting tumour size assessed after 4 weeks. 'Tissue site' indicates the site where cells were implanted, and 'cells injected' indicates whether the cells injected were derived from a primary tumour or liver metastasis (liver met). Relative weights of tumour and associated normal tissue compared with normal tissue of age-matched mice, or tumour weight in the subcutaneous flank, are shown. $n = 4$ mice were used for the pancreas injection; $n = 3$ mice were used for the liver and subcutaneous injections; $n = 5$ mice were used for the normal tissue weights. Male mice were used for all the comparisons. Data are the mean ± s.d. *$P = 0.0479$; NS, not significant. **c,d**, The percentage of cells that stained positive for Ki67 by immunohistochemistry was quantified in tissue sections from tumours arising from primary pancreatic cancer or liver metastatic cells implanted into the pancreas or liver as indicated (**c**) or implanted into the pancreas or lung as indicated (**d**). Data from $n = 4$ (pancreas), $n = 3$ (liver; primary cells) or $n = 5$ (liver; liver met) mice are shown in **c**; Data are from $n = 3$ (pancreas) or $n = 3$ (lung) mice in **d**. Ki67 percentage = number of positive stained cells in each image field divided by the total number of cells in the same field multiplied by 100. One representative field per tumour was analysed; mean ± s.d. is shown. **e**, The percentage of cells stained positive for BrdU as assessed by immunohistochemistry was quantified in tissue sections from tumours arising from primary or metastatic cells in either the pancreas or the liver as indicated; each data point represents one region of a tumour obtained from $n = 2$ (pancreas; primary cells), $n = 3$ (pancreas; liver met), $n = 1$ (liver, primary) or $n = 2$ (liver; liver met) mice per group. Quantification was determined by manually counting number of positive cells divided by the total number of cells in the same field multiplied by 100; *$P = 0.0109$; mean ± s.d. is shown. **f,g**, The percentage of cells that stained positive for cleaved caspase-3 by immunohistochemistry was quantified on tissue sections derived from tumours arising from either primary or metastatic cells in either the pancreas or liver (**f**) or in tumours arising from primary or metastatic cells in either the pancreas or the lung (**g**). Each data point indicates an average of three regions from each mouse ($n = 3$ mice per group). Percentage positivity was quantified by manually counting number of positive cells divided by the total number of cells in the same field multiplied by 100; *$P = 0.0154$. Data are the mean ± s.d. **h**, Relative weights of tumours derived from equal numbers of cancer cells implanted into nude (NU/J) mice after 4 weeks and associated normal tissue weights from age-matched mice is shown. $n = 4$ (normal tissues) and $n = 3$ (cells injected in pancreas and liver) mice per group; both male and female mice were used. Data are the mean ± s.d. *$P = 0.0150$, ***$P = 0.0003$. **i,j**, The indicated number of cancer cells derived from a primary pancreatic tumour (P), or liver metastases (M) were implanted into either the pancreas (**i**) or the liver (**j**), and animals were followed to determine if a tumour formed as well as how long mice with tumours survived after implantation; male mice were used for all the conditions. The number of mice with tumours is shown, with the total number of mice injected for each number of cells indicated in parentheses. These data were also used to calculate an approximate tumour-initiating capacity for primary-derived and metastasis-derived cells at each tissue site: Pancreas, primary (1/63.4), liver met (1/99.2), P value = 0.531; Liver, primary (1/417), liver met (1/2005), P value = 0.106. Statistical significance was determined using the ELDA (extreme limiting dilution analysis) software. **k**, Equal numbers of cancer cells isolated from primary pancreatic tumours or paired liver or lung metastases arising in the KPC mouse model were implanted into the pancreas, liver, lung (via tail vein) or subcutaneous space, and resulting tumour size assessed after 4 weeks. As in **b**, relative weights of tumour and associated normal tissue compared with normal tissue of age-matched mice, or tumour weight in the subcutaneous flank, are shown. 'Cells injected' indicates whether the cells injected were derived from a primary tumour, liver or lung metastasis. $n = 3$ (all normal tissues), $n = 4$ (pancreas; primary cells), $n = 4$ (pancreas; liver met), $n = 5$ (pancreas; lung met) and $n = 3$ (lung, liver, and subcutaneous tissue sites injected with cells) mice per group. Data are the mean ± s.d. Pancreas (**$P = 0.0045$); liver (primary versus normal liver, *$P = 0.0263$; liver met versus normal liver, *$P = 0.0383$); lung (liver met versus normal lung, ****$P < 0.0001$; lung met versus normal lung, **$P = 0.0050$). Comparisons between groups were made using a two-tailed Student's t-test (**b**–**h** and **k**).

Fig. 4f and Supplementary Table 3). Further, tumours formed from primary-derived or lung metastasis-derived cells showed similar staining for proliferation and cell death markers when growing in the lung or the pancreas (Fig. 2d,g and Extended Data Fig. 5b,c,e,g). These data argue that cells from PDAC lung metastases also retain a preference to grow in the primary site.

Propagation of cancer cells in metastatic sites can select for cancer cells that seed a particular tissue site, and studying these cells has revealed metabolic differences between primary and metastatic tumours[33–35]. However, it remains unclear whether cells selected to seed metastatic sites also improves their ability to grow once they arrive at that site. To answer this later question, cells derived from lung or liver metastases in KPC mice were propagated by three rounds of repeated implantation and passaging in the lung or liver, respectively (Fig. 3a and Extended Data Fig. 8a). Consistent with published results[33,34], lung metastatic cancer cells selected for in this manner efficiently formed lung tumours when injected via the tail vein (Extended Data Fig. 8b), and natural lung metastases developed in mice when these cells were

implanted in the pancreas (Extended Data Fig. 8c). These same properties were also present in the parental cells derived from a natural lung metastasis (Extended Data Fig. 8b,c), which are otherwise infrequent in KPC mice[21]. Of note, spontaneous lung metastases were never observed from primary-derived or liver metastasis-derived cells implanted into either the pancreas or the liver. Propagating liver metastatic cancer cells as liver tumours resulted in tumours with larger tumour area when the cells were implanted in the liver compared to parental liver metastatic cells, and enabled liver tumour formation when injected via the tail vein (Extended Data Fig. 8d,e). Liver metastases were not observed following tail vein injection of parental cells derived from liver metastases or primary-derived or lung metastasis-derived cells, confirming that passaging PDAC cells in the liver results in an increased ability to seed new liver tumours as reported in other contexts[33].

When the ability to form tumours in different tissue sites was quantitatively assessed over a defined time window, the liver-selected and lung-selected cells still formed larger tumours in the pancreas (Fig. 3b–e and Extended Data Fig. 8f). Again, cells derived from both
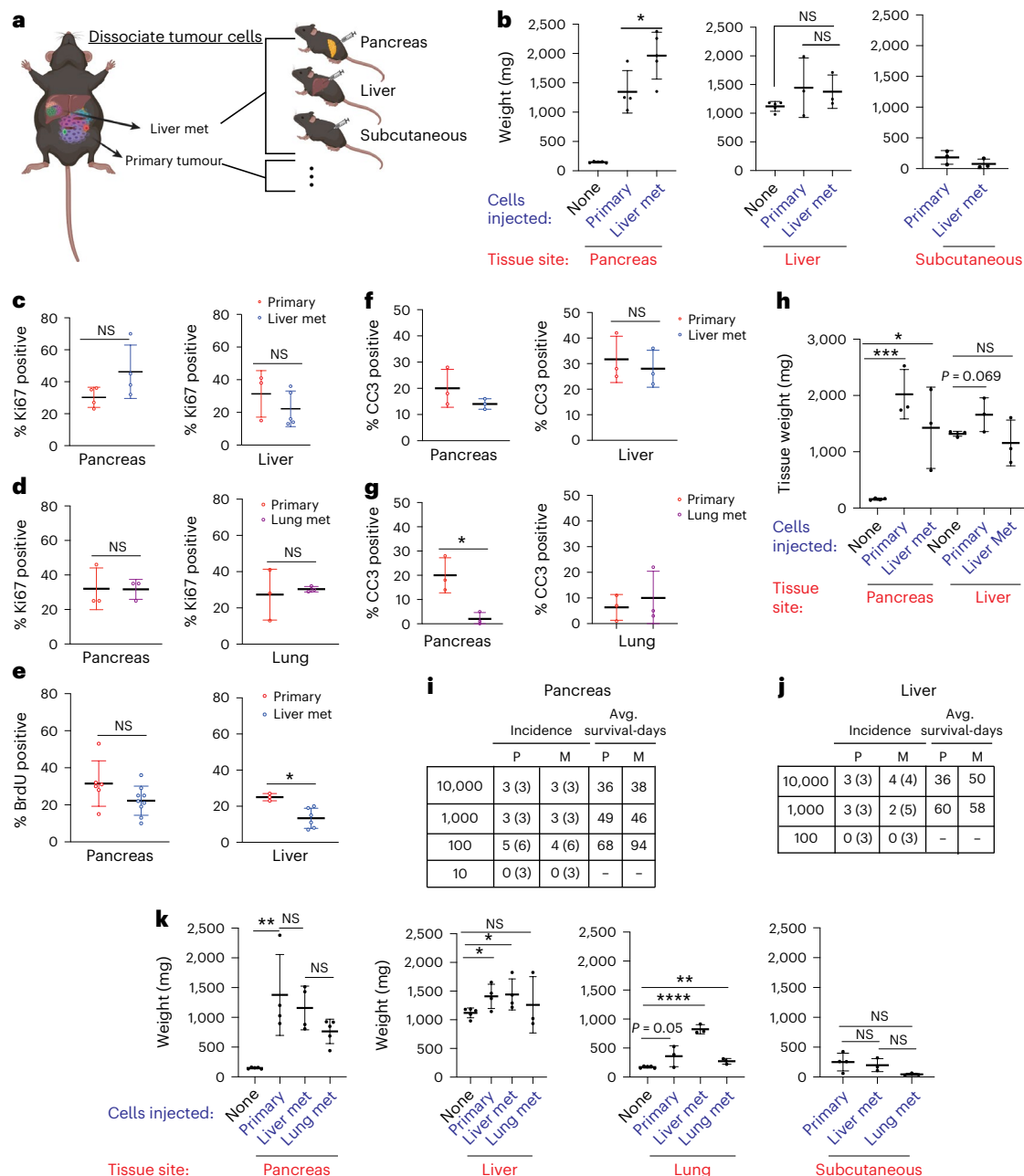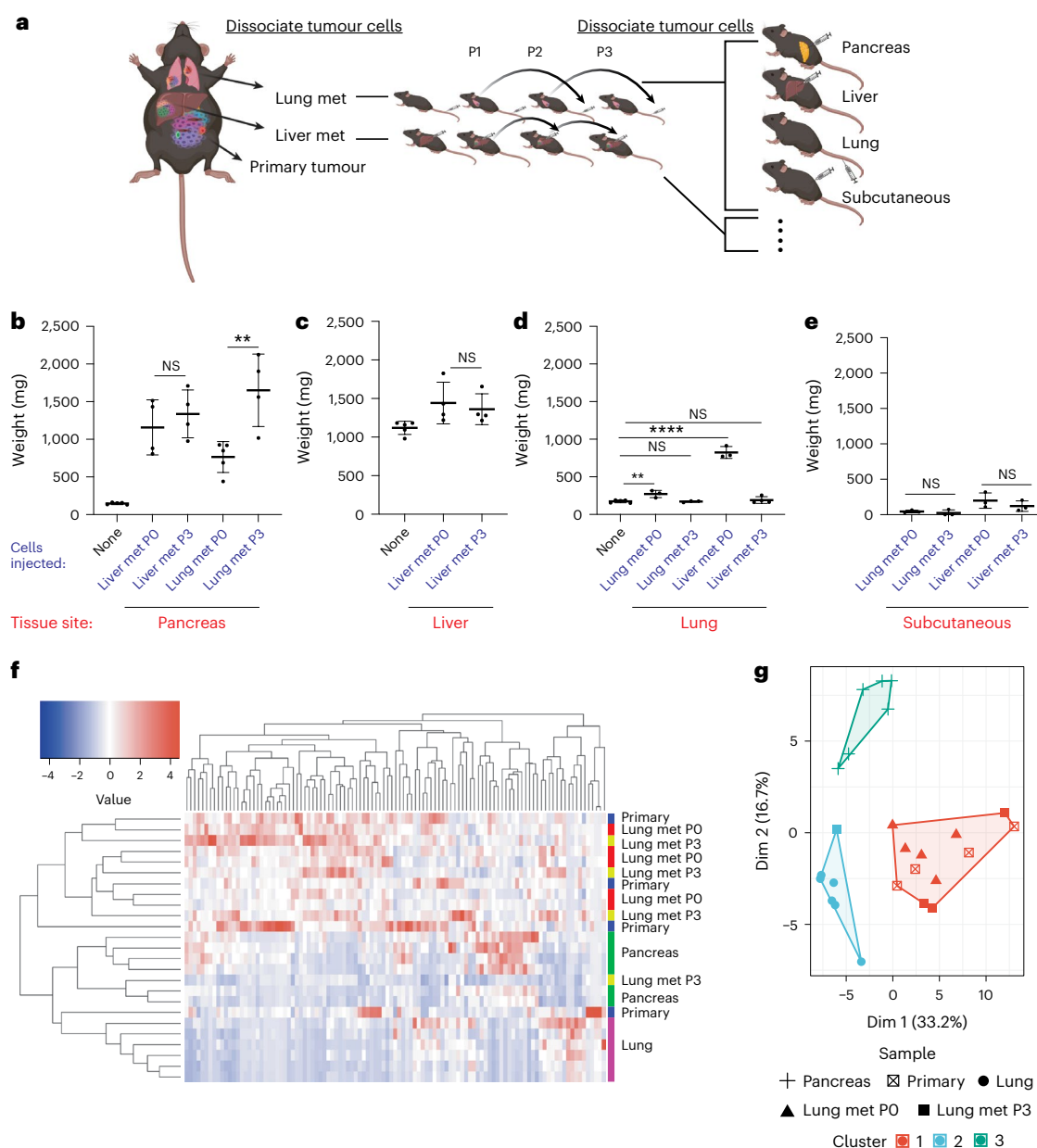
Fig. 3 | Pancreatic cancer cells retain metabolic phenotypes found in the primary tumour even when repeatedly passaged in a metastatic site.
a, Schematic depicting propagation of lung and liver pancreatic cancer metastases arising in KPC mice by implantation into the lung or liver to form tumours three times before use in transplantation experiments to quantitatively assess proliferation and metabolic phenotypes in different tissue sites. Created with BioRender.com. **b**–**e**, Equal numbers of cancer cells isolated from primary pancreatic tumours, paired liver or lung metastases (P0), or liver or lung metastatic cancer cells that were passaged in the liver or lung as described in **a** (P3) were implanted into the pancreas, liver, lung (via tail vein) or subcutaneous space, and resulting tumour size assessed after 3 weeks. Relative weights of tumour and associated normal tissue compared with normal tissue of age-matched mice, or tumour weight in the subcutaneous flank, is shown.

'Cells injected' indicates whether the cells injected were derived from a P0 or P3 liver or lung metastasis. Data are the mean ± s.d.; pancreas (**$P = 0.0070$), lung (**$P = 0.00499$, ****$P < 0.0001$); $n = 3$ (subcutaneous site), $n = 3$ (lung site; all except liver met P3 ($n = 4$)), $n = 5$ (all normal tissues); $n = 4$ (liver site) and $n = 4$ (pancreas site–all except lung met P0 ($n = 5$)) mice per group. **f**,**g**, Relative metabolite levels arising in tumours from primary, P0 and P3 lung metastases cells implanted in the pancreas were assessed by liquid chromatography–mass spectrometry. Metabolite levels were also measured for normal pancreas and lung tissue from age-matched wild-type mice. The metabolite data for each sample were clustered in two different ways: unsupervised clustering represented as a heat map (**f**) or k-means unsupervised clustering (**g**). Comparisons between groups were made using a two-tailed Student's t-test (**b**–**e**).

liver and lung metastases were able to form tumours at all sites, with the largest tumours forming in the pancreas and the smallest in the flank. Notably, similar-sized tumours were observed at each site regardless of where the cells were derived from, and whether they were passaged previously as tumours in the liver or lung. These data support a model where pancreatic cancer cells retain a preference to grow in the primary site, even when repeatedly passaged in a metastatic tissue site.

We next examined whether propagation of tumour cells in different tissues alters their metabolic phenotype. We first examined metabolites extracted from tumours that were generated from cells derived from spontaneous lung metastases (Passage 0: P0) and from cells derived from in vivo selected lung metastases (Passage 3: P3) and compared those to metabolites extracted from primary pancreatic tumours and age-matched normal lung or normal pancreas tissue.

The small size of tumours that formed in the lung prevented assessment of metabolites when tumours are growing in that site; however, we could assess metabolites extracted from the large tumours that formed in the pancreas to determine whether propagating cells in the lung stably selects for tumours with major alterations in metabolism as these cells retain an ability to spontaneously reseed lung metastases (Extended Data Fig. 8c). Unsupervised clustering revealed that tumours generated from lung metastases, spontaneous or selected, cluster based on metabolite levels with the primary tumour (Fig. 3f and Supplementary Table 4). When the same dataset was clustered using unsupervised k-means clustering, one tumour derived from passaging of cancer cells in the lung clustered with the normal lung while the remaining tumour samples clustered together (Fig. 3g). These data suggest that passaging cancer cells as tumours in the lung, for the most part, does not select for extensive stable alterations in metabolism that are retained when these cells are grown in the pancreas, although these data do not argue there are no metabolite differences present between tumours and normal tissues.

To assess whether a preference for cancer cells to form tumours in the pancreas is explained by the pancreas being more permissive to tumour growth, we asked whether cancer cells derived from different cancers also have a preference to grow in the pancreas relative to their primary tissue site. First, we considered primary lung adenocarcinoma (LUAD) cells derived from the *LSL-Kras^G12D/+; Trp53^fl/fl; Ad-Cre* mouse model[36]. Primary LUAD cells did not grow well as tumours in the pancreas, yet these cells formed large tumours in the lungs of syngeneic mice (Fig. 4a). This preference to grow in the lung relative to the pancreas was the opposite of what we observed with PDAC lung metastasis-derived cells (Fig. 3b,d and Extended Data Fig. 8g). We next considered whether direct cancer cell delivery into the lung had the same phenotype as initiating lung tumours via tail vein injection. We delivered the same number of primary LUAD cells or PDAC lung metastasis-derived cells via intratracheal injection and observed after a fixed time that primary LUAD-derived cells formed more nodules than PDAC lung metastasis-derived cells (Fig. 4b and Extended Data Fig. 8h). Next, we injected the same number of primary LUAD cells or primary PDAC cancer cells directly into the lung parenchyma and observed that after a fixed time the primary LUAD-derived cells give rise to larger tumours than PDAC cells (Extended Data Fig. 8i,j).

To assess whether hepatocellular carcinoma (HCC)-derived cells have a preference to grow in the liver relative to the pancreas, a fixed number of mouse HCC cells[37,38] were implanted into the pancreas or liver of syngeneic mice, and tumour burden was assessed after 4 weeks.

While there was some variability between mice, HCC cells implanted into the liver trended towards larger tumours relative to tumours that formed in the pancreas even after accounting for normal tissue weight (Fig. 4c and Extended Data Fig. 8k). However, the same number of HCC-derived cells formed larger tumours over a fixed period of time in the liver than PDAC liver metastasis-derived cells (Fig. 3b,c and Extended Data Fig. 8k). HCC and LUAD do not typically metastasize to the pancreas, but do metastasize to the lung and liver, respectively. Thus, we next asked whether primary HCC and primary LUAD cells retain a preference to grow in their respective primary tissue sites relative to the lung or liver. When a fixed number of primary LUAD cells are transplanted into the liver or delivered to the lung, we observe that after a fixed time the LUAD cells form larger tumours in the lung than they do in the liver (Fig. 4d, Extended Data Fig. 9a and Supplementary Table 5). Similarly, the HCC cells form larger tumours in the liver than they do in the lung (Fig. 4e, Extended Data Fig. 9b and Supplementary Table 5). These data support a model where cancer cells from different origins retain a preference to grow in their tissue of origin relative to a metastatic site.

To begin to test whether tissue nutrient availability differences contribute to the preference of cancer cells to grow in their primary site, we measured the absolute concentrations of metabolites in interstitial fluid isolated from normal mouse tissues as well as matched plasma[10]. The concentrations of most metabolites in tissue interstitial fluid were lower than those measured in plasma, and levels of nutrients present in interstitial fluid differed across tissue sites (Extended Data Fig. 9c and Supplementary Table 6). Next, we formulated media to match the nutrient levels measured in plasma or interstitial fluid from each tissue site and assessed the ability of cells to proliferate in these media relative to standard DMEM-based or RPMI-based culture media. We found that primary PDAC cells, PDAC liver metastasis-derived cells and PDAC lung metastasis-derived cells proliferated at similar rates in standard media or media with plasma nutrient condition (Fig. 4f). While proliferation was slower in media formulated to match nutrient levels measured in tissues, the PDAC primary-derived and metastasis-derived cells proliferated at similar rates in media with pancreas nutrient levels but fail to expand in the time frame assayed in media with lung or liver nutrient conditions. While we were unable to expand any cells in media with liver interstitial fluid nutrient levels, media with lung interstitial nutrient levels can support proliferation of some cancer cells. Both primary mouse LUAD cells as well as established A549 human lung cancer cells proliferate in lung interstitial fluid nutrient conditions in contrast to PDAC lung metastasis-derived cells (Extended Data Fig. 9d). While these

Fig. 4 | Tissue of origin influences the metabolism and tissue site preference for metastatic tumour growth. a, Equal numbers of LUAD cells derived from the *LSL-Kras^G12D/+; Trp53^fl/fl; Ad-Cre* mouse model were implanted into the pancreas or delivered to the lung and resulting tumour size assessed after 4 weeks. Relative weights of tumour and associated normal tissue compared with normal tissue from age-matched mice are shown. Data are the mean ± s.d.; *$P < 0.05$, ****$P < 0.0001$; $n = 5$ (normal tissues) and $n = 3$ (for both pancreas and lung sites) mice per group. **b**, Equal number of cells derived from pancreatic lung metastasis (lung met) or from primary lung cancer described in **a** were introduced into the lung via intratracheal inhalation of the cancer cells; tumour burden in the lung is depicted as the number of lung nodules in each section of three mice per group. Each data point represents one mouse. Data are the mean ± s.d.; *$P < 0.05$. **c**, Equal numbers of RIL-176 HCC cells were implanted into the pancreas or the liver and resulting tumour size assessed after 4 weeks. Relative weights of tumour and associated normal tissue compared with normal tissue from age-matched mice are shown. $n = 3$ (liver primary cells; pancreas), $n = 3$ (liver primary cells; liver) and $n = 5$ (normal tissues) mice were used. Data are the mean ± s.d.; *$P < 0.05$. Comparisons between groups were made using a two-tailed Student's *t*-test. **d**, Equal numbers of primary lung cancer cells described in **a** were implanted into the liver or delivered to the lung via tail vein injection and tumour area determined via analysis of histological sections after 4 weeks. Each data point represents one mouse and three mice were used per tissue site. Data are the

mean ± s.d. **$P < 0.005$. Comparisons between groups were made using a two-tailed Student's *t*-test (**a**–**d**). **e**, Equal numbers of primary HCC cells described in **c** were implanted into the liver or delivered to the lung via tail vein injection and tumour area in each site was quantified as in **d** after 4 weeks; $n = 3$ mice were used per tissue site. **f**, Proliferation rate of primary pancreatic, liver or lung metastatic cells in either standard cell culture media (DMEM, RPMI) or in media formulated to match the metabolite concentrations measured in normal mouse plasma or in mouse tissue (pancreas, liver or lung) interstitial fluid. Representative data from three biological replicates from at least $n = 2$ independent experiments per line for each condition are shown. Data are the mean ± s.d. **g,h**, Uniform manifold approximation and projection (UMAP) plot comparing metabolic gene expression in single cells from primary PDAC, lung metastases and liver metastases from the KPC model (**g**); and the UMAP plot of metabolic gene expression analysis in **g** with each clonal population represented; these clones are arbitrarily labelled as clones 1–6 and do not match clone numbers in the original publication (**h**). **i**, Cross-correlation analysis of bulk metabolic gene expression profiles involving 3,240 genes from 620 samples with gene expression obtained from The Cancer Genome Atlas (TCGA) HCC, PDAC (Panc-seq) or TCGA PDAC data (top). Ranked metastatic samples with a high degree of hepatocyte contamination as assessed by higher gene expression of hepatocyte markers and lower gene expression of ductal markers are shown on the bottom with corresponding correlation to normal liver.

data should not be interpreted to suggest that the relative levels of all nutrients found in each site determine how well cancer cells can grow in each site, they support a model wherein primary tissue nutrient levels in aggregate better support proliferation of cancer cells that arise in that tissue than nutrient levels found in metastatic sites.

To further examine whether metastatic tumours retain some metabolic phenotypes found in primary tumours, we queried an available single-cell RNA-sequencing (scRNA-seq) dataset to determine whether metabolic gene expression is conserved between KPC mouse PDAC primary tumours, liver metastases and lung metastases[27] and found overlap in metabolic gene expression between primary PDAC and

liver metastases when all cells were analysed (Extended Data Fig. 10a). When we restricted the analysis to the most abundant clonal populations represented in the dataset, we found evidence for heterogeneity in metabolic gene expression among the cancer cells; however, this heterogeneity was similar in cells derived from both the primary and metastatic sites with the caveat that very few cells derived from lung metastases were available for analysis (Fig. 4g,h and Extended Data Fig. 10b). In this dataset, barcoded cancer cells were implanted into the pancreas and traced across tissues[27]. When metabolic gene expression analysis was performed based on the barcoded clones, cells that clustered by barcode did not segregate by tissue site (Fig. 4g,h and
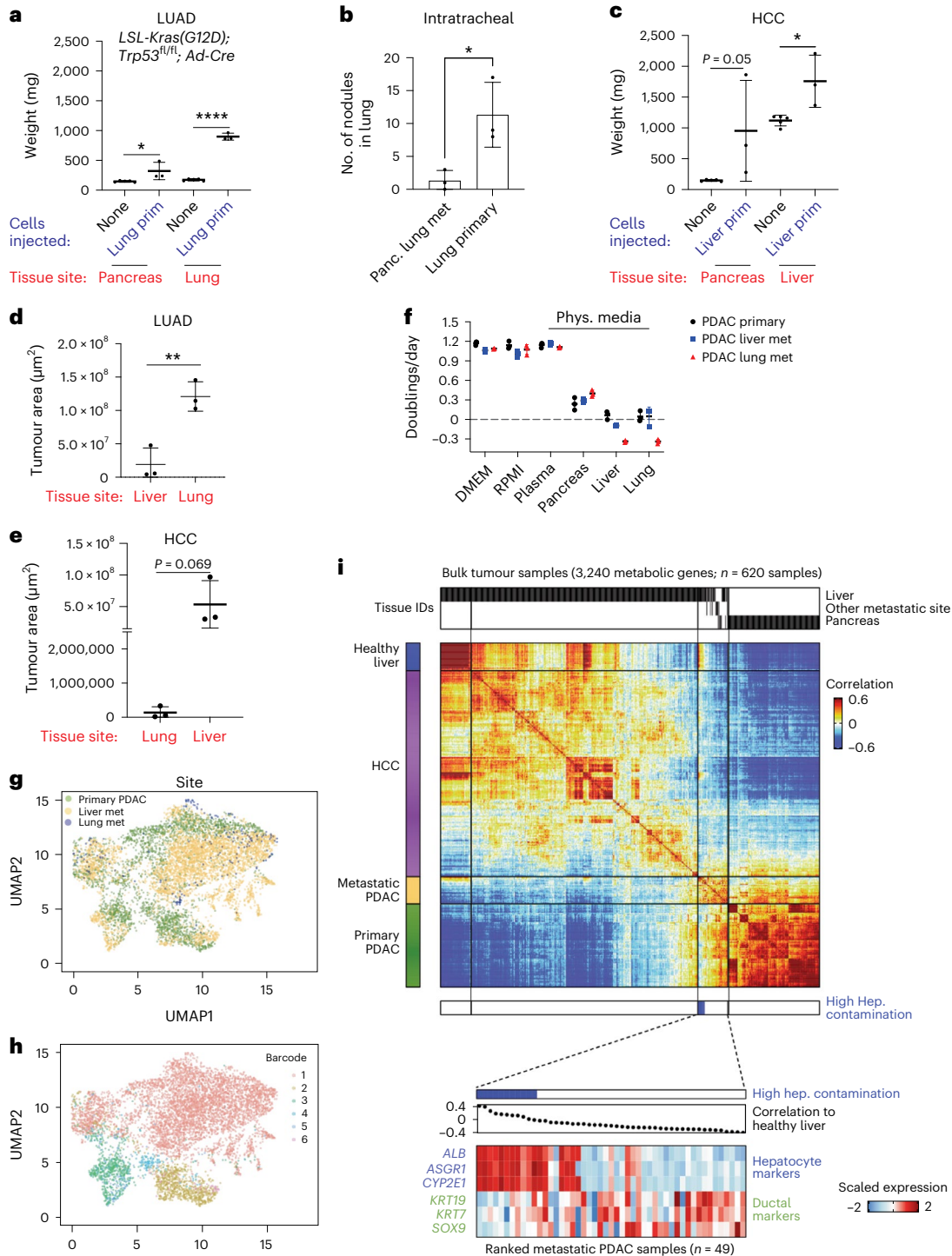
Extended Data Fig. 10c). Thus, metabolic heterogeneity in the PDAC cells from this dataset is driven more by clonal relationships between cells than by the tissue environment where the cells were found. That is, these data argue that despite heterogeneity in metabolic gene expression among pancreatic cancer cells isolated from each tissue site, and metabolic heterogeneity among cancer cell clones, we did not find evidence for selection of a clone defined by a specific global metabolic gene expression pattern in metastases. Rather, these data suggest that PDAC cancer cells arising in KPC mice retain a similar global metabolic gene expression programme regardless of site, although they do not argue against specific metabolic adaptations being associated with tumour growth in a particular site.

To assess whether these same findings related to metabolic gene expression are found in human cancers, we analysed expression of metabolic genes from available PDAC and HCC human tumour-derived RNA-seq datasets[39,40]. Consistent with tissue of origin having a stronger influence on global metabolic gene expression than tissue site, we found overlap of metabolic gene expression between primary and liver metastatic PDAC, and that this metabolic gene expression is distinct from that observed in primary HCC, which overlaps with normal liver tissue (Fig. 4i and Extended Data Fig. 10d,e). Notably, the human PDAC liver metastases that overlapped most with primary HCC and liver samples contained a higher degree of contamination with normal hepatocytes as determined by higher expression of hepatocyte markers (Fig. 4i and Extended Data Fig. 10d,e). These data further support a model wherein metastatic cancer cells retain aspects of the primary tumour metabolic programme, and that this may constrain cancer cell proliferation in metastatic tissue sites.

That aspects of the metabolic programme found in metastases are shared with those found in the primary tumour argues that the metabolic programme cancer cells use to support proliferation is in part defined by the tissue of origin even when exposed to a new metastatic tissue environment. These data do not rule out some phenotypes being selected that enable cancer cells to proliferate in metastatic sites. There is evidence that specific metabolic adaptions can promote cancer growth in specific tissues[12,41–45]; however, the metabolic plasticity of cancer cells appears to be less flexible than often assumed[14]. Rather, that cancers prefer to grow in the primary site supports a model wherein inflexible aspects of a metabolic programme derived from the cancer tissue of origin might limit the nutrient environments where cancer cells can grow. It is unlikely that cancer cells retain preferences for all nutrients found in the primary tissue, yet a relative lack of metabolic plasticity may explain why chemotherapies that target metabolism remain effective in treating both primary and metastatic tumours with patients selected for treatment based on the cancer tissue of origin. Moreover, this model may underlie, at least in part, why particular cancer types metastasize to stereotyped locations, as accessing a nutrient environment with enough similarity to the primary tumour may be necessary to support aspects of the metabolic programme retained from the primary tumour. Nevertheless, there is limited evidence from small numbers of patients that metastases from primary renal cell cancer, breast cancer and colorectal cancer exhibit faster radiographic progression than primary tumours or have increased Ki67 staining compared to the primary tumour[46,47]. Radiographic progression of individual lesions is often observed in patients with later-stage cancers and could be influenced by multiple factors including prior therapies. Metastases to contralateral unaffected healthy tissue that matches the primary site are observed in some cancers, such as lung cancer, but are not common in other cancers such as breast cancer. Whether some cancer types exhibit more extensive metabolic adaptation after metastases than the pancreatic, lung and hepatocellular cancers considered here remains unknown. Regardless, better understanding the impact of different tissue nutrient environments on proliferation of cancers arising in different sites could inform treatment selection for patients based on the pattern of metastasis for a given primary tumour.

Methods

Animal studies

All studies were approved by the Massachusetts Institute of Technology (MIT) Committee on Animal Care (protocol no. 0119-001-22). Both male and female animals were used. For autochthonous models, $Kras^{G12D/+}$; $Trp53^{R172H/+}$; $Pdx1$-Cre (KPC)[21] and $Kras^{G12D/+}$; $Trp53^{R172H/+}$; $Pdx1$-Cre; LSL-$tdTomato$ (KPCT)[29] mice from a mixed 129/Sv and C57BL6/J background as well as a pure C57BL6/J genetic background were used for most experiments. For the experiments involving immunocompromised mice, both male and female 8–10-week-old nude mice (NU/J) obtained from the Jackson Laboratory were used. Both male and female C57BL6/J mice were used for all other transplantation experiments. For metabolomics, normal tissue was isolated from age-matched 6-month-old mice, while tumours and paired liver metastases were isolated from the same 6–8-month-old animals. All tissues were isolated at the same time of day. Animals were housed under a 12-h light–dark cycle and co-housed with littermates with ad libitum access to water and food, except following surgical procedures, where animals were singly housed to comply with Animal Care protocols. Animals were never allowed to exceed the maximal tumour burden as established by the MIT Committee on Animal Care and were euthanized after any signs of distress.

Sample sizes for animal studies were selected using preliminary experiments involving pancreas tumour implants. We calculated that a minimum sample size of two mice per group could detect a statistically significant difference based on a priori power analysis using G*Power software with an effect size, d, of 9.835, an alpha of 0.05 and a power of 0.80. For experiments where cells were injected into the liver, we calculated that a sample size of three mice per group would be sufficient to obtain an effect size of 3.452 with an alpha of 0.05 and a power of 0.80. For the lung transplant experiments, we calculated that three mice per group could achieve an effect size of 5.1583, an alpha of 0.05 and a power 0.80. For subcutaneous tumour experiments, we calculated that a sample size of three mice per group could achieve an effect size of 3.957 with an alpha of 0.05 and a power of 0.80. Experiments were designed with at least three mice per condition. No randomization was used in the data collection process. No animals were excluded from any experiment.

Tumour transplantation

Mice aged approximately 6–8 weeks (for C57B16/J) or 8–10 weeks (for Nu/J) were injected with 100,000 cells PDAC cells derived from primary or metastatic tumours arising in KPC or KPCT mice at the indicated site. Cells were delivered into the pancreas as previously published[29]. To introduce cells into the liver, after anaesthetization, a small incision was introduced to exteriorize one lobe of the liver, and cells were directly injected into the liver. Mice were monitored for recovery and appropriate postoperative care was provided. To deliver cancer cells to the lung via the circulation, 100,000 cells were injected into the tail vein. Mice were euthanized 4 weeks after tumour cell injection or at signs of distress. All mice within the same experimental group were euthanized at the same time point. For direct ultrasound-guided implantation into the lung parenchyma, 10,000 cells were injected into 18-week-old male C57BL6/J mice. In brief, mice were first depilated and imaged by microCT (Skyscan 1276 X-ray microtomograph (Bruker)) in the pronated position to obtain three axis coordinates for injection in the left lung using distances from the liver–lung interface, pleural line and the skin. Animals were then transferred in the pronated position to the Vevo3100 ultrasound imager (FujiFilm-VisualSonics), and the three landmarks by ultrasound imaging combined with a precision driver mounted syringe allowed for 2 μl focal delivery of cell suspension to the lung. Mice were euthanized 3 weeks after tumour cell injection. For intratracheal delivery of cancer cells into lungs, a previously published protocol[36] was used where anaesthetized mice were placed on a platform suspended by their front teeth such that the chest was

vertical. A light source was used for visualization and a catheter (Clint, CP-26746) was guided into the open trachea allowing 50 µl cell suspension in HBSS (100,000 cells) delivery. Inhalation was confirmed based on disappearance of the liquid in the catheter.

Limiting dilution studies to assess tumour initiation
Mice were injected with the indicated number of cells and monitored twice a week for signs of tumour burden. The tumour-initiating capacity was calculated using ELDA software (http://bioinf.wehi.edu.au/software/elda/). At least three mice were included for each condition.

Cell competition experiments
Pancreatic cancer cells derived from primary, or liver metastatic tumours engineered to express either mCherry or GFP were mixed in equal numbers and pre-injection representation was confirmed using flow cytometry (BD LSR II). In total, 100,000 cells containing the mixed population were injected into the pancreas, liver, or subcutaneously, and after tumours formed, they were excised, digested and analysed by flow cytometry to determine relative tumour representation. The percentage of fluorescently labelled cancer cells is reported relative to all cell types within the tumour and, therefore, the total percentage of fluorescently labelled cells does not equal 100%. Alternatively, tumour tissue was obtained and fixed for histology and a representation of mCherry- or GFP-expressing cells was assessed by immunohistochemistry.

Tumour adaptation to grow in the lung or liver
Cells from naturally arising liver and lung metastatic tumours in the KPC mouse model were isolated and cultured for less than ten population doublings. Cells from lung metastases were transplanted into the lung via tail vein injection. Resulting tumours were dissociated and re-transplanted into secondary recipient mice without in vitro propagation. This process was repeated three times. A similar approach was taken for liver metastases where cells were implanted in the liver, with resulting tumours dissociated and re-transplanted in secondary recipient mice without in vitro propagation three times. Mice were euthanized at different time points based on established and approved criteria, and following the last round of in vivo selection, tumours were dissociated and cultured for less than five population doublings before use in transplantation experiments (P0 refers to the parental cells (before in vivo adaptation); P3 refers to the tumour and tumour cells derived from three rounds of in vivo adaptation) as indicated.

Cell isolation and cell culture
Cells were isolated from primary and metastatic mouse pancreatic tumours as described previously[29,48]. Briefly, tumours were exteriorized, minced and digested with Collagenase XI (Sigma, C9407) and Dispase II (Roche, 04942078001) and plated in DMEM. RIL-175 mouse HCC cells were isolated by the Duda Laboratory from hepatic tumours arising in C57BL/6 mice as previously described[38]. LUAD cells were obtained from *LSL*-Kras(G12D); *Trp53*^fl/fl^;*Ad-Cre* lung cancer mice as previously described[49]. Cells were cultured in DMEM (Corning, 10-013-CV) supplemented with 10% heat-inactivated FBS. Penicillin–streptomycin was added only at the time of cell isolation from mice. Cells were regularly tested for mycoplasma using the MycoAlert Plus kit (Lonza). All cell lines (when first derived) were verified using an antibody to detect the p.Gly12Asp *Kras* mutation (Cell Signaling, 14429). For some cell lines, the p.Gly12Asp *Kras* mutation was also verified by Sanger Sequencing and, where applicable, by fluorescent TdTomato expression.

Cell proliferation
In total, 30,000 cells were plated in six-well plates in 2 ml of DMEM with 10% FBS and cultured for at least 12 h. Cells were washed once, and medium was replaced with fresh DMEM at the time of cell counting on

day 0 and day 3 using a Cellometer Auto T4 Plus Cell Counter (Nexcelom Bioscience), and doublings per day was calculated using the formula: proliferation rate (doublings/day) = $\log_2$(final cell count (day 3)/initial cell count (day 0))/3 (days).

Isotope labelling experiments in cultured cells
Cells were plated in six-well plates and the next day cells were washed three times with warm PBS, and DMEM without glucose and pyruvate supplemented with 10% dialysed FBS and 10 mM [U-^{13}C]glucose (Cambridge Isotope Laboratories) was added for 24 h before metabolite extraction.

Isotope labelled nutrient infusion experiments in mice
[U-^{13}C]glucose or [U-^{13}C]glutamine (Cambridge Isotope Laboratories) infusion into control or tumour-bearing mice was performed as previously described[29,50]. Three weeks after implantation of cancer cells, animals underwent surgical catheter implantation in the jugular vein 3–4 days before labelled glucose infusion. Mice were fasted for 4 h before infusion and animals remained conscious and mobile for the duration of the infusion. Labelled glucose was delivered at a rate of 0.4 mg min^{-1} for 6 h; then plasma and tumour tissue were isolated, and flash frozen for mass spectrometry analysis. Labelled glutamine was delivered at a rate of 3.7 mg per kg body weight per minute for 6 h. All isotope labelling experiments in mice were performed at the same time of day.

BrdU incorporation in tumours
BrdU (10 mg ml^{-1} in PBS) was injected intraperitoneally into mice in 200 µl per 20 g of mouse body weight. Twenty-four hours after injection, tumours and associated normal tissue were collected and fixed in 10% formalin before immunohistochemistry staining with anti-BrdU antibody (Abcam, ab6326) at a dilution of 1:2,000 in PBS.

Metabolite extraction
To analyse glucose in plasma, 10 µl of plasma was extracted with 100% methanol, dried under nitrogen, and derivatized with 50 µl of 2 wt% hydroxylamine hydrochloride (2% Hox) in pyridine followed by incubation at 90 °C for 60 min. Next, 100 µl of propionic anhydride was added, and samples incubated at 60 °C for 30 min, followed by evaporation under nitrogen at room temperature overnight. The next day, dried samples were dissolved in 100 µl of ethyl acetate and transferred to glass vials for analysis by gas chromatography–mass spectrometry (GC–MS). For tissue metabolite analysis, harvested tissues were rinsed in ice-cold blood blank saline and flash frozen in liquid nitrogen. Frozen tissues were ground into a powder using a pre-chilled mortar and pestle. Tissue powder was weighed into pre-chilled tubes and extracted with methanol (containing 500 nM each of 17 isotopically labelled ^{13}C/^{15}N amino acids (Cambridge Isotope Laboratories)):chloroform:water (6:3:4 vol/vol/vol), vortexed for 10 min and centrifuged for 10 min at maximum speed. Polar metabolites were transferred to microcentrifuge tubes, dried under nitrogen and resuspended in different volumes of water containing labelled non-standard amino acid mix (Cambridge Isotope Laboratories, MSK-NCAA-1) to account for differences in starting tissue weight. For cultured cells, cells were seeded at 30,000 cells per well in a six-well dish in 2 ml of medium and incubated for 72 h, or 100,000 cells were plated and incubated overnight. The medium was aspirated from cells before a rapid wash in ice-cold bank saline followed by addition of 500 ml ice-cold 80% methanol in water containing 500 nM each of 17 isotopically labelled ^{13}C/^{15}N amino acids (Cambridge Isotope Laboratories). Alternatively, for metabolite analysis by GC–MS, cells were extracted in equal parts 80% methanol (containing 2.5 ng ml^{-1} norvaline internal standard) and chloroform. Samples were vortexed 10 min at 4 °C and spun at 16,000 g for 10 min at 4 °C. An equal volume of the polar fraction was transferred to a new tube and dried under nitrogen and frozen at −80 °C before analysis by mass spectrometry.

Isolation of tissue interstitial fluid

Mouse tissue interstitial fluid and plasma was collected using an adapted published protocol[10]. Organs from five male mice fed an ad libitum diet were pooled and combined per isolation, which was done for three different groups for a total of 15 mice. Each pooled sample was treated as an individual data point for the liquid chromatography–mass spectrometry measurements and analysis. In each group, the age of the mice ranged from 6 to 8 weeks (cohort 1), and 8 weeks (cohorts 2 and 3). All mice were euthanized at the same time of day. Tissues were kept on ice throughout the harvest and, when ready to pool, were briefly rinsed in ice-cold saline and excess liquid was removed before tissues were placed in a 50 ml conical vial lined with a 20-μm nylon mesh filter (Spectrum Labs, 148134). The samples were spun at 400g for 10 min, flow-through collected, and spun again at 400g before storage in −80 °C until further analysis. Absolute metabolite concentrations were determined as published[10]. Data represent micromolar (μM) metabolite concentrations.

Formulation of media to match tissue metabolites

To generate media reflecting the average of metabolite concentrations measured in tissue interstitial fluid and plasma, individual metabolites were weighed and combined into different pools; and pools were further combined to generate base media. The complete medium comprised base medium supplemented with 10% dialysed serum. Any metabolite that was not measured in our analysis was substituted with prior measured concentrations found in mouse plasma and kept consistent across media.

Gas chromatography–mass spectrometry

GC–MS was used to analyse metabolites as previously described[29]. Briefly, dried metabolite extracts were dissolved in 16 ml methoxamine reagent (Thermo Fisher, TS-45950) and incubated at 37 °C for 90 min. In total, 20 ml N-methyl-N-(tert–butyldimethylsilyl) trifluor-oacetamide + 1% tert–Butyldimethylchlorosilane (Sigma, 375934) was added to the sample and incubated at 60 °C for 1 h. Samples were centrifuged for 5 min, and 20 ml of the derivatized sample was transferred to GC–MS vial for analysis using a DB-35MS column (Agilent Technologies, 122-3832) installed in an Agilent 7890 gas chromatograph coupled to an Agilent 5975C mass spectrometer. The helium carrier gas was used at a constant flow rate of 1.2 ml min^{-1}. One microliter of the sample was injected at 270 °C. After injection, the GC–MS oven was held at 100 °C for 1 min, increased to 300 °C at 3.5 °C min^{-1}. The oven was then ramped up to 320 °C at 20 °C min^{-1} and held for 5 min at 320 °C. The mass spectrometry system operated under electron impact ionization at 70 eV and the mass spectrometry source and quadrupole was held at 230 °C and 150 °C, respectively. The detector was used in scanning mode and the scanned ion range was 100–650 m/z. Total ion counts were determined by integrating appropriate ion fragments for each metabolite using EI-MAVEN software (Elucidata).

Liquid chromatography–mass spectrometry

Metabolite profiling was conducted on a QExactive bench top orbitrap mass spectrometer equipped with an Ion Max source and a HESI II probe, which was coupled to a Dionex UltiMate 3000 HPLC system (Thermo Fisher Scientific). External mass calibration was performed using the standard calibration mixture every 7 days. Typically, samples were reconstituted in 50 μl water and 2 μl was injected onto a SeQuant ZIC-pHILIC 150 × 2.1-mm analytical column equipped with a 2.1 × 20-mm guard column (both 5-mm particle size; EMD Millipore). Buffer A was 20 mM ammonium carbonate, 0.1% ammonium hydroxide, and buffer B was acetonitrile. The column oven and autosampler tray were held at 25 °C and 4 °C, respectively. The chromatographic gradient was run at a flow rate of 0.150 ml min^{-1} as follows: 0–20 min, linear gradient from 80–20% B; 20–20.5 min, linear gradient form 20–80% B; 20.5–28 min, hold at 80% B. The mass spectrometer was operated in

full-scan, polarity-switching mode, with the spray voltage set to 3.0 kV, the heated capillary held at 275 °C, and the HESI probe held at 350 °C. The sheath gas flow was set to 40 units, the auxiliary gas flow was set to 15 units, and the sweep gas flow was set to 1 unit. MS data acquisition was performed in a range of m/z = 70–1,000, with the resolution set at 70,000, the AGC target at $1 × 10^6$, and the maximum injection time at 20 ms. Relative quantification of polar metabolites was performed with TraceFinder 4.1 (Thermo Fisher Scientific) using a mass tolerance of 5 ppm and referencing an in-house library of chemical standards. Data were filtered according to predetermined quality-control (QC) metrics: coefficient of variance of pools < 25%; R of linear dilution series < 0.975. Data were normalized to cell number from a separately plated set of samples collected at the time of metabolite extraction.

For untargeted metabolomics, data were acquired as described above, with data-dependent MS^2 data collected on pooled samples using a top-10 method, with stepped collision energies of 15, 30 and 45 V. The resolution was set at 17,500, the automatic gain control (AGC) target was $2 × 10^5$, the max injection time (IT) was 100 ms, and the isolation window was set at 1.0 m/z. Data were analysed using Compound Discoverer 3.1 (Thermo Fisher Scientific) and by including an in-house mass-list. P values were adjusted according to the Benjamini–Hochberg method.

Flow cytometry

Tumours were dissected, minced and digested at 37 °C for 30 min with 1 mg ml^{-1} Collagenase I (Worthington Biochemical, LS004194), 3 mg ml^{-1} Dispase II (Roche, 04942078001) and 0.1 mg ml^{-1} DNase I (Sigma, D4527) in 5 ml PBS. After 30 min, cells were incubated with 10 mM EDTA at room temperature for 5 min. Cells were filtered through a 70-mm cell strainer, washed twice in PBS, and resuspended in flow cytometry staining buffer (Thermo Fisher, 00-4222-57) for fluorescent protein expression analysis on a BD LSR II flow cytometer. At least 10,000 cells were analysed per sample.

Immunohistochemistry

Tissue was fixed in formalin for at least 24 h. Sections from formalin-fixed paraffin embedded tissues were stained using antibodies against mCherry (1:500 dilution; Novus Biologicals, NBP1-96752), GFP (1:250 dilution; Novus Biologicals, NB600-308), pan-cytokeratin (1:500 dilution; Abcam, ab133496), Ki67 (1:250 dilution; Novus Biologicals, NB110-89717), BrdU (1:2,000 dilution; Abcam, ab6326) or cleaved caspase-3 (Asp175; 1:400 dilution; Cell Signaling, 9661). Antibodies were diluted in 10% normal goat serum diluted at a 1:2 ratio (Thermo Fisher, 50062Z) in PBS-T.

Histology and image analysis

Histology sections were scanned using Aperio Digital Scanning and imported into web-based Aperio eSlide Manager or into QuPath software. Image analysis was done using Fiji or QuPath software. The tumour area and total area were calculated for all sections, and the net tumour area was calculated by dividing the tumour area by the total area. The number of nodules in the lung was calculated manually. Tumour histology grade was assessed using clinical criteria by a gastrointestinal pathologist (O.H.Y.). The histological grade assessment of the adenocarcinoma was based on the following criteria: grade 1: well-differentiated (greater than 95% of tumour composed of glands); grade 2: moderately differentiated (50–95% of tumour composed of glands); grade 3: poorly differentiated (49% or less of tumour composed of glands).

Analysis of mouse tumour RNA-seq data

Metabolic gene expression analysis of mouse tumours used pancreatic tumour scRNA-seq data from a published source[27]. Principal component analysis plots depict analysis of metabolic genes from entire cell populations. For mouse scRNA-seq data analysis, after normalizing

to total counts, metabolic genes were analysed from primary, liver or lung metastases and UMAP plots for the most abundant samples were generated using scanpy version 1.8.0 to determine overlap between gene expression across tissue sites. For single-cell analysis, lineage tracing of the most represented cell clones from the study permitted analysis of individual clonal populations and UMAP plots depict overlap between gene expression across overrepresented clones within the tumour across different tissue sites. Pearson correlation was also found between pairs of single cells using the scores for the top 20 principal components.

Analysis of human tumour RNA-seq data

FASTQ files for bulk RNA expression profiles were downloaded from the relevant repository (TCGA, https://toil.xenahubs.net; Metastatic PDAC, dbGaP study accession phs001652.v1.p1), and all data were processed using the same pipeline. Briefly, each sample's sequences were marked for duplicates and then mapped to hg38 using STAR. After running QC checks using RNAseqQC, gene-level count matrices were generated using RSEM. Instructions to run the pipeline are given in the Broad CCLE GitHub repository via https://github.com/broadinstitute/ccle_processing/. Length-normalized values (TPM) were then transformed according to $\log_2(TPM + 1)$ for downstream analysis. We then scaled and centred the entire dataset to allow relative comparisons across sample types (normal Liver, HCC, PDAC and metastatic PDAC). We tested whether metastatic PDAC more closely resembles the metabolic state of the primary site (pancreas) or the dominant metastatic tissue of residence (liver) and used normal liver and HCC profiles as relevant comparators. To do this, we trimmed the expression data to 3,240 metabolically associated genes using a literature-curated list. We then performed a cross-correlational analysis (Pearson's r) across all samples and separated this matrix by study after clustering (Ward's method). We then generated similarity scores for each metastatic sample ($n = 49$) by computing their average Pearson's r to primary PDAC, HCC or normal liver samples.

Statistical analysis

Results are represented as the mean ± s.d. unless otherwise specified. Statistical analysis was performed using GraphPad Prism (version 9.1.1). Where multiple comparisons were appropriate, a two-way ANOVA statistical test was used and statistical significance between multiple comparisons was determined using Tukey's multiple-comparisons test available in GraphPad Prism Software Analysis tools. The statistical significance between two groups was calculated using an unpaired two-tailed student t-test where noted. Data were not formally tested but were assumed to be normally distributed. Data collection and analysis were performed blind to the conditions of the experiment.

Reporting summary

Further information on research design is available in the Nature Portfolio Reporting Summary linked to this article.

Data availability

Source data are provided with this paper. Any associated Extended Data Figures and Supplementary Tables are provided.

References

1. Yang, D. et al. Lineage tracing reveals the phylodynamics, plasticity, and paths of tumor evolution. *Cell* **185**, 1905–1923 (2022).
2. Celià-Terrassa, T. & Kang, Y. Distinctive properties of metastasis-initiating cells. *Genes Dev.* **30**, 892–908 (2016).
3. Boutin, A. T. et al. Oncogenic *Kras* drives invasion and maintains metastases in colorectal cancer. *Genes Dev.* **31**, 370–382 (2017).
4. Makohon-Moore, A. P. et al. Limited heterogeneity of known driver gene mutations among the metastases of individual patients with pancreatic cancer. *Nat. Genet.* **49**, 358–366 (2017).
5. Muir, A. & Vander Heiden, M. G. The nutrient environment affects therapy. *Science* **360**, 962–963 (2018).
6. Abbott, K. L. et al. Screening in serum-derived medium reveals differential response to compounds targeting metabolism. *Cell Chem. Biol.* **30**, 1156–1168 (2023).
7. Altea-Manzano, P., Cuadros, A. M., Broadfield, L. A. & Fendt, S. Nutrient metabolism and cancer in the in vivo context: a metabolic game of give and take. *EMBO Rep.* **21**, e50635 (2020).
8. Mayers, J. R. et al. Tissue of origin dictates branched-chain amino acid metabolism in mutant *Kras*-driven cancers. *Science* **353**, 1161–1165 (2016).
9. Yuneva, M. O. et al. The metabolic profile of tumors depends on both the responsible genetic lesion and tissue type. *Cell Metab.* **15**, 157–170 (2012).
10. Sullivan, M. R. et al. Quantification of microenvironmental metabolites in murine cancers reveals determinants of tumor nutrient availability. *Elife* **8**, e44235 (2019).
11. Reinfeld, B. I. et al. Cell-programmed nutrient partitioning in the tumour microenvironment. *Nature* **593**, 282–288 (2021).
12. Ferraro, G. B. et al. Fatty acid synthesis is required for breast cancer brain metastasis. *Nat. Cancer* **2**, 414–428 (2021).
13. Schild, T., Low, V., Blenis, J. & Gomes, A. P. Unique metabolic adaptations dictate distal organ-specific metastatic colonization. *Cancer Cell* **33**, 347–354 (2018).
14. Lehúede, C., Dupuy, F., Rabinovitch, R., Jones, R. G. & Siegel, P. M. Metabolic plasticity as a determinant of tumor growth and metastasis. *Cancer Res.* **76**, 5201–5208 (2016).
15. Bartman, C. R. et al. Slow TCA flux and ATP production in primary solid tumours but not metastases. *Nature* **614**, 349–357 (2023).
16. Basnet, H. et al. Flura-seq identifies organ-specific metabolic adaptations during early metastatic colonization. *Elife* **8**, e43627 (2019).
17. Piskounova, E. et al. Oxidative stress inhibits distant metastasis by human melanoma cells. *Nature* **527**, 186–191 (2015).
18. Gaude, E. & Frezza, C. Tissue-specific and convergent metabolic transformation of cancer correlates with metastatic potential and patient survival. *Nat. Commun.* **7**, 13041 (2016).
19. Hu, J. et al. Heterogeneity of tumor-induced gene expression changes in the human metabolic network. *Nat. Biotechnol.* **31**, 522–529 (2013).
20. Fidler, I. J. The pathogenesis of cancer metastasis: The 'seed and soil' hypothesis revisited. *Nat. Rev. Cancer* **3**, 453–458 (2003).
21. Hingorani, S. R. et al. Trp53R172H and KrasG12D cooperate to promote chromosomal instability and widely metastatic pancreatic ductal adenocarcinoma in mice. *Cancer Cell* **7**, 469–483 (2005).
22. Kim, M. Y. et al. Tumor self-seeding by circulating cancer cells. *Cell* **139**, 1315–1326 (2009).
23. Gejman, R. S. et al. Rejection of immunogenic tumor clones is limited by clonal fraction. *Elife* **7**, e41090 (2018).
24. Obenauf, A. C. & Massagué, J. Surviving at a distance: organ-specific metastasis. *Trends Cancer* **1**, 76–91 (2015).
25. Maddipati, R. & Stanger, B. Z. Pancreatic cancer metastases harbor evidence of polyclonality. *Cancer Discov.* **5**, 1086–1097 (2015).
26. Lambert, A. W., Pattabiraman, D. R. & Weinberg, R. A. Emerging biological principles of metastasis. *Cell* **168**, 670–691 (2017).
27. Simeonov, K. P. et al. Single-cell lineage tracing of metastatic cancer reveals selection of hybrid EMT states. *Cancer Cell* **39**, 1150–1162 (2021).
28. Elia, I., Doglioni, G. & Fendt, S. M. Metabolic hallmarks of metastasis formation. *Trends Cell Biol.* **28**, 673–684 (2018).
29. Lau, A. N. et al. Dissecting cell-type-specific metabolism in pancreatic ductal adenocarcinoma. *Elife* **9**, e56782 (2020).

30. Ariston Gabriel, A. N. et al. Differences between KC and KPC pancreatic ductal adenocarcinoma mice models, in terms of their modeling biology and their clinical relevance. *Pancreatology* **20**, 79–88 (2020).

31. Pérez-Mancera, P. A., Guerra, C., Barbacid, M. & Tuveson, D. A. What we have learned about pancreatic cancer from mouse models. *Gastroenterology* **142**, 1079–1092 (2012).

32. Faubert, B., Solmonson, A. & DeBerardinis, R. J. Metabolic reprogramming and cancer progression. *Science* **368**, eaaw5473 (2020).

33. Yamaguchi, N. et al. PCK1 and DHODH drive colorectal cancer liver metastatic colonization and hypoxic growth by promoting nucleotide synthesis. *Elife* **8**, e52135 (2019).

34. Minn, A. J. et al. Genes that mediate breast cancer metastasis to lung. *Nature* **436**, 518–524 (2005).

35. Bos, P. D. et al. Genes that mediate breast cancer metastasis to the brain. *Nature* **459**, 1005–1009 (2009).

36. DuPage, M., Dooley, A. L. & Jacks, T. Conditional mouse lung cancer models using adenoviral or lentiviral delivery of Cre recombinase. *Nat. Protoc.* **4**, 1064–1072 (2009).

37. Kapanadze, T. et al. Regulation of accumulation and function of myeloid derived suppressor cells in different murine models of hepatocellular carcinoma. *J. Hepatol.* **59**, 1007–1013 (2013).

38. Zender, L. et al. Generation and analysis of genetically defined liver carcinomas derived from bipotential liver progenitors. *Cold Spring Harb. Symp. Quant. Biol.* **70**, 251–261 (2005).

39. Raphael, B. J. et al. Integrated genomic characterization of pancreatic ductal adenocarcinoma. *Cancer Cell* **32**, 185–203 (2017).

40. Aguirre, A. J. et al. Real-time genomic characterization of advanced pancreatic cancer to enable precision medicine. *Cancer Discov.* **8**, 1096–1111 (2018).

41. Schug, Z. T. et al. Acetyl-CoA synthetase 2 promotes acetate utilization and maintains cancer cell growth under metabolic stress. *Cancer Cell* **27**, 57–71 (2015).

42. Elia, I. et al. Breast cancer cells rely on environmental pyruvate to shape the metastatic niche. *Nature* **568**, 117–121 (2019).

43. Rinaldi, G. et al. In Vivo evidence for serine biosynthesis-defined sensitivity of lung metastasis, but not of primary breast tumors, to mTORC1 inhibition. *Mol. Cell* **81**, 386–397 (2021).

44. Elia, I. et al. Proline metabolism supports metastasis formation and could be inhibited to selectively target metastasizing cancer cells. *Nat. Commun.* **8**, 15267 (2017).

45. Chi, Y. et al. Cancer cells deploy lipocalin-2 to collect limiting iron in leptomeningeal metastasis. *Science* **369**, 276–282 (2020).

46. Klein, C. A. Parallel progression of primary tumours and metastases. *Nat. Rev. Cancer* **9**, 302–312 (2009).

47. Oda, T. et al. Growth rates of primary and metastatic lesions of renal cell carcinoma. *Int. J. Urol.* **8**, 473–477 (2001).

48. Boj, S. F. et al. Organoid models of human and mouse ductal pancreatic cancer. *Cell* **160**, 324–338 (2015).

49. Gocheva, V. et al. Quantitative proteomics identify Tenascin-C as a promoter of lung cancer progression and contributor to a signature prognostic of patient survival. *Proc. Natl Acad. Sci. USA* **114**, E5625–E5634 (2017).

50. Davidson, S. M. et al. Environment impacts the metabolic dependencies of ras-driven non-small cell lung cancer. *Cell Metab.* **23**, 517–528 (2016).

Acknowledgements

Author contributions

S.S.: conceptualization, investigation, visualization, methodology, writing—original draft, writing—review and editing. Y.G., P.S.W., S.Y.V., K.L.A., A.J., F.G., K.M.T., L.V.D., B.T.D., K.C., T.K., A.N.L., A.M.D. and C.A.L.: methodology, investigation, writing—review and editing. S.M., D.G.D., L.M., N.H., V.S., D.J.I. and O.H.Y.: methodology. D.V., B.M.W., A.K.S. and A.J.A.: supervision. M.G.V.H.: conceptualization, supervision, visualization, funding acquisition, project administration, methodology, writing—original draft, writing—review and editing.

Competing interests

M.G.V.H. is a scientific advisor for Agios Pharmaceuticals, iTeos Therapeutics, Faeth Therapeutics, Sage Therapeutics, Lime Therapeutics, Pretzel Therapeutics and Auron Therapeutics. A.N.L. is a current employee of Pfizer. K.C. is a current employee of Thermo Fisher Scientific. D.G.D. is a consultant for Innocoll and has research grants from Exelixis, Bayer, BMS and Surface Oncology. A.J.A. has consulted for Anji Pharmaceuticals, Affini-T Therapeutics, Arrakis Therapeutics, AstraZeneca, Boehringer Ingelheim, Kestrel Therapeutics, Merck & Co., Inc., Mirati Therapeutics, Nimbus Therapeutics, Oncorus, Inc., Plexium, Quanta Therapeutics, Revolution Medicines, Reactive Biosciences, Riva Therapeutics, Servier Pharmaceuticals, Syros Pharmaceuticals, T-knife Therapeutics, Third Rock Ventures and Ventus Therapeutics; holds equity in Riva Therapeutics and Kestrel Therapeutics; and has research funding from AstraZeneca, Boehringer Ingelheim, Bristol Myers Squibb, Deerfield, Inc., Eli Lilly, Mirati Therapeutics, Nimbus Therapeutics, Novartis, Novo Ventures, Revolution Medicines and Syros Pharmaceuticals. The other authors declare no competing interests.

Additional information

Extended data is available for this paper at https://doi.org/10.1038/s42255-024-01105-9.

Supplementary information The online version contains supplementary material available at https://doi.org/10.1038/s42255-024-01105-9.

Correspondence and requests for materials should be addressed to Matthew G. Vander Heiden.

Peer review information *Nature Metabolism* thanks the anonymous reviewers for their contribution to the peer review of this work. Primary Handling Editor: Alfredo Giménez-Cassina, in collaboration with the *Nature Metabolism* team.

Reprints and permissions information is available at www.nature.com/reprints.

[1]Koch Institute for Integrative Cancer Research, Massachusetts Institute of Technology, Cambridge, MA, USA. [2]Department of Biology, Massachusetts Institute of Technology, Cambridge, MA, USA. [3]Department of Medical Oncology, Dana-Farber Cancer Institute, Boston, MA, USA. [4]Broad Institute of MIT and Harvard, Cambridge, MA, USA. [5]Institute for Medical Engineering and Science, Massachusetts Institute of Technology, Cambridge, MA, USA. [6]Department of Systems Biology, Columbia University Medical Center, New York, NY, USA. [7]Department of Biochemistry and Molecular Biology, University of Massachusetts Amherst, Amherst, MA, USA. [8]Whitehead Institute for Biomedical Research, Cambridge, MA, USA. [9]Edwin L Steele Laboratories, Department of Radiation Oncology, Massachusetts General Hospital and Harvard Medical School, Boston, MA, USA. [10]Department of Medicine, Brigham and Women's Hospital and Harvard Medical School, Boston, MA, USA. [11]Preclinical Imaging and Testing Facility, Massachusetts Institute of Technology, Cambridge, MA, USA. [12]Department of Biological Engineering, Massachusetts Institute of Technology, Cambridge, MA, USA. [13]Howard Hughes Medical Institute, Chevy Chase, MD, USA. [14]Ragon Institute of MGH, MITnd Harvard, Cambridge, MA, USA. [15]Department of Pathology, Massachusetts General Hospital and Beth Israel Deaconess Medical Center and Harvard Medical School, Boston, MA, USA. [16]Program in Molecular Medicine, University of Massachusetts Chan Medical School, Worcester, MA, USA. [17]Department of Biomedical Informatics, Columbia University Medical Center, New York, NY, USA. [18]Department of Chemistry, Massachusetts Institute of Technology, Cambridge, MA, USA. [19]These authors contributed equally: Yetis Gultekin, Peter S. Winter, Sidney Y. Vermeulen, Konstantine M. Tchourine. ✉e-mail: mvh@mit.edu
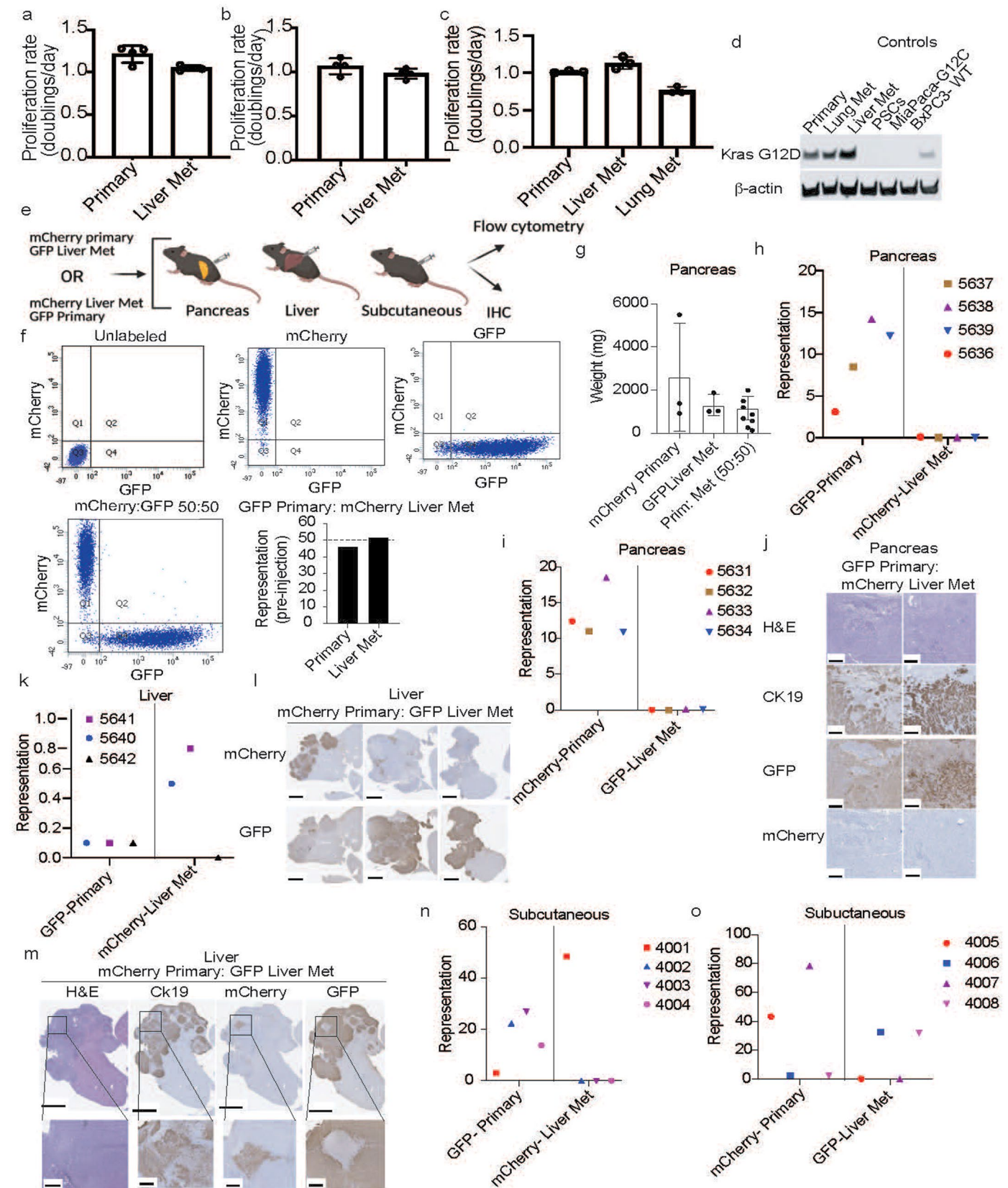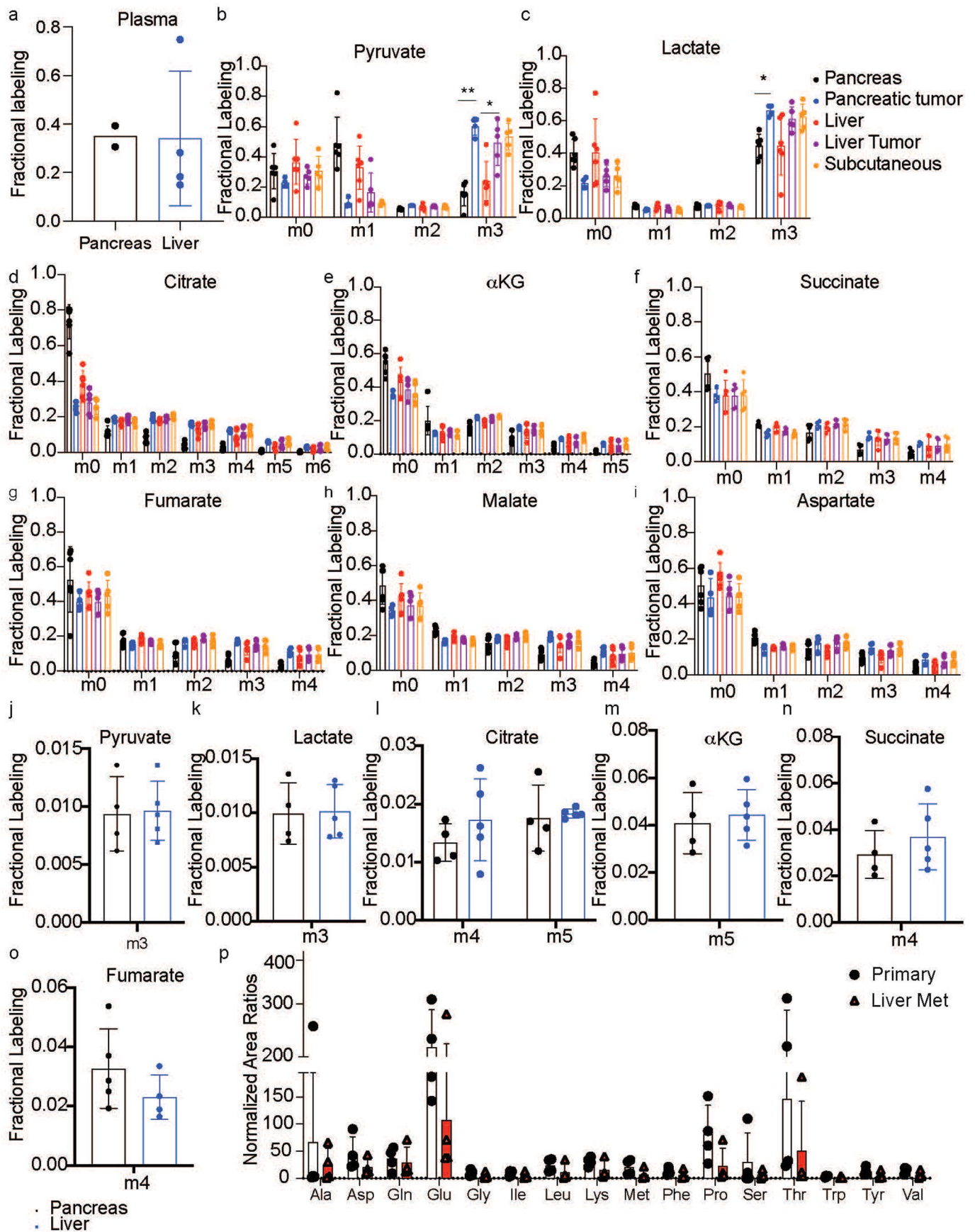
Extended Data Fig. 1 | See next page for caption.

Extended Data Fig. 1 | Proliferation of primary and metastatic pancreatic cancer cells in culture and cell competition experiments in mice.
(a-c) Proliferation rate (doublings/day) of cells in culture that were isolated from primary tumors, or from liver or lung metastases, as indicated. Data shown were obtained from three independently derived paired cell lines; mean +/− stdev, n=4 technical replicates (a and b), or 3 technical replicates (c) per cell line; representative data from independent biological replicates of at least n=3 per cell line. (d) Representative western blot analysis assessing mutant Kras expression in protein lysates obtained from the indicated pancreatic cell lines and established human cell line controls and pancreatic stellate cells (PSCs). Mutant Kras G12D expression was only validated once per cell line at the time of generating the cell lines. (e) Schematic of experimental procedure where primary or liver metastatic pancreatic cancer cells (liver met) labeled with mCherry or GFP were injected into the pancreas, liver, or subcutaneous flank; either implanted individually or as a 50:50 mixture of the indicated cells. Representation of each cell population in the final tumor was analyzed by flow cytometry or by immunohistochemistry (IHC). Created with BioRender.com. (f) Flow cytometry of individually labeled cell populations (top) and a mixed population (bottom left). Approximately equal representation of each labeled cancer cell population in a mixed population was confirmed prior to injection (representative data shown bottom right). (g) Tumor weight post injection of individually labeled cancer cells (n=3) or a mixed cell population containing equal numbers of both primary (prim) and liver metastasis (met)-derived pancreatic cancer cells (n=8). Mean +/− stdev. (h) Representation of GFP-labeled primary or mCherry-labeled liver metastatic cells in a tumor derived from injection of a mixed population containing equal numbers of labeled primary and liver metastasis-derived pancreatic cancer cells into the pancreas as determined by flow cytometry. Each data point represents one mouse; the numbers associated with each mouse indicate animal ID with each animal being injected with the same mixed population of cells. (i) Representation of mCherry-labeled primary or GFP-labeled liver metastatic cells in a tumor derived from injection of a mixed population containing equal numbers of labeled primary and liver metastasis-derived pancreatic cancer cells into the pancreas as determined by

flow cytometry. Each data point represents one mouse; the numbers associated with each mouse indicate animal ID with each animal being injected with the same mixed population of cells. (j) Immunohistochemistry to assess GFP and mCherry expression in a tumor derived from injection of a mixed population containing equal numbers of primary and liver metastasis-derived pancreatic cancer cells into the pancreas as in (h) Scale bar, 250 μm. (k) Representation of GFP-labeled primary or mCherry-labeled liver metastatic cells in a tumor derived from injection of a mixed population containing equal numbers of primary and metastasis-derived pancreatic cancer cells into the liver as determined by flow cytometry. Each data point represents one mouse; the numbers associated with each mouse indicate animal ID with each animal being injected with the same mixed population of cells. (l) Immunohistochemistry to assess GFP and mCherry expression in three different tumors derived from injection of a mixed population containing equal numbers of a primary and liver metastasis-derived pancreatic cancer cells into the liver as in (k), although the mixed population of cells were from an independent experiment where the primary tumor cells were labeled with mCherry, and the liver metastasis cells were labeled with GFP. Scale bar, ~2500 μm. (m) Immunohistochemistry to assess GFP, mCherry, or Cytokeratin-19 (Ck19) expression in whole mount liver tissue sections from a mouse from an independent experiment where a mixed population containing equal numbers of primary, and liver metastasis-derived pancreatic cancer cells were implanted into the liver as in (m). (n) Representation of GFP-labeled primary or mCherry-labeled liver metastatic cells in a tumor derived from subcutaneous injection of mixed population containing equal numbers of labeled primary and liver metastasis-derived pancreatic cancer cells into the flank. Each data point represents one mouse; the numbers associated with each mouse indicate animal ID with each animal being injected with the same mixed population of cells. (o) Representation of mCherry-labeled primary or GFP-labeled liver metastatic cells in a tumor derived from subcutaneous injection of mixed population containing equal numbers of labeled primary and liver metastasis-derived pancreatic cancer cells into the flank. Each data point represents one mouse; the numbers associated with each mouse indicate animal ID with each animal being injected with the same mixed population of cells.

Extended Data Fig. 2 | See next page for caption.

Extended Data Fig. 2 | Assessment of glucose and glutamine fate and amino acid levels in primary pancreatic tumors and liver metastases. (**a**) Plasma enrichment of U[13]C-glucose as determined by GC-MS after a 6-hour U[13]C-glucose infusion at a rate of 0.4 mg/min[29] in mice with a primary pancreatic tumor (pancreas; n=2 female mice) or with a liver metastatic pancreatic tumor (liver; n=4 female mice). (**b-i**) Fractional labeling of each indicated metabolite in the indicated tissue harvested from aged-matched control mice (pancreas, liver) or from mice harboring a primary pancreatic tumor, a subcutaneous pancreatic tumor, or a liver metastatic tumor that was infused with U[13]C-glucose as measured by GC-MS. In all cases tumors were generated by implanting pancreatic cancer cells derived from a primary tumor arising in the KP$^{-/-}$C model. Mean +/− stdev; **p= 0.0088, *p=0.0224 (panel b); *p=0.0237; n.s.- not significant.

Comparisons between groups were made using a two-tailed Student's *t*-test (b and c). n=6 mice were used for the normal tissues (both pancreas and liver), n=4 mice were used for the pancreatic tumor, n=5 mice were used for the liver tumor, and n=5 mice were used for the subcutaneous tumors. (**j-o**) Fractional labeling of each indicated metabolite in pancreatic cancer primary or liver metastasis tumors as measured by GC-MS following a 6-hour infusion of U[13]C-glutamine at a rate of 3.7 mg/kg/min into mice. In all cases tumors were generated by implanting pancreatic cancer cells derived from a primary tumor arising in the KP$^{-/-}$C mouse model. Mean +/− stdev; n=4 mice/group. (**p**) Levels of amino acids measured by LC-MS from primary pancreatic tumors and matched liver metastases arising in KPC mice; Mean +/− stdev (n=4 mice/condition).
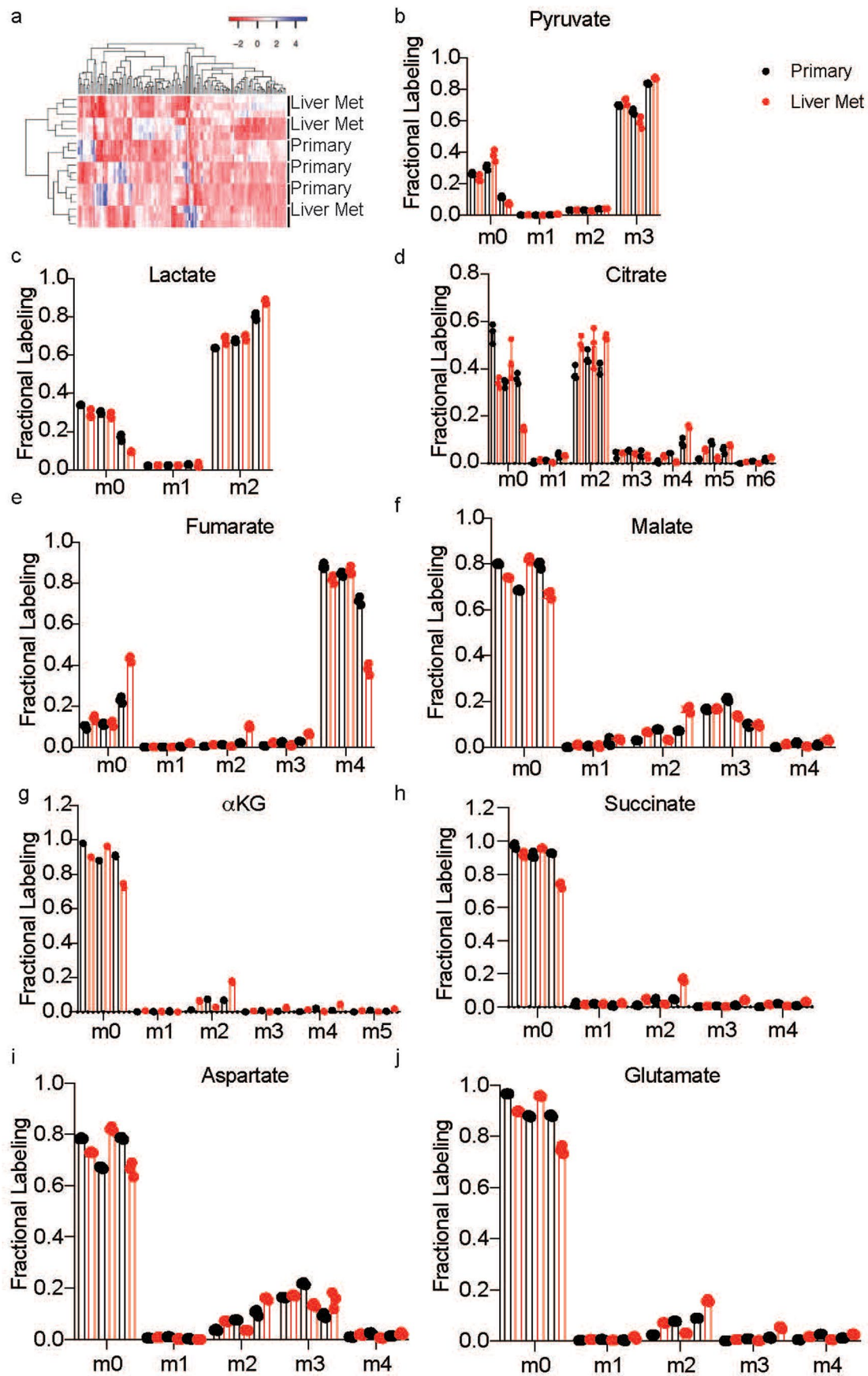
Extended Data Fig. 3 | See next page for caption.

Extended Data Fig. 3 | Metabolic characterization of primary pancreatic cancer and liver metastatic cells in culture. (a) Heatmap representation of unsupervised clustering of relative metabolite levels measured by LC-MS from paired primary and liver metastatic cells cultured in standard DMEM conditions; data is shown in triplicate per cell line from three independently derived cell lines. (b-j) Fractional labeling of each indicated metabolite in cells derived from a primary pancreatic tumor or a liver metastasis after being cultured with U-^{13}C glucose for 24 hours. mean +/− stdev; data is shown from three independently derived cell lines; n=3.
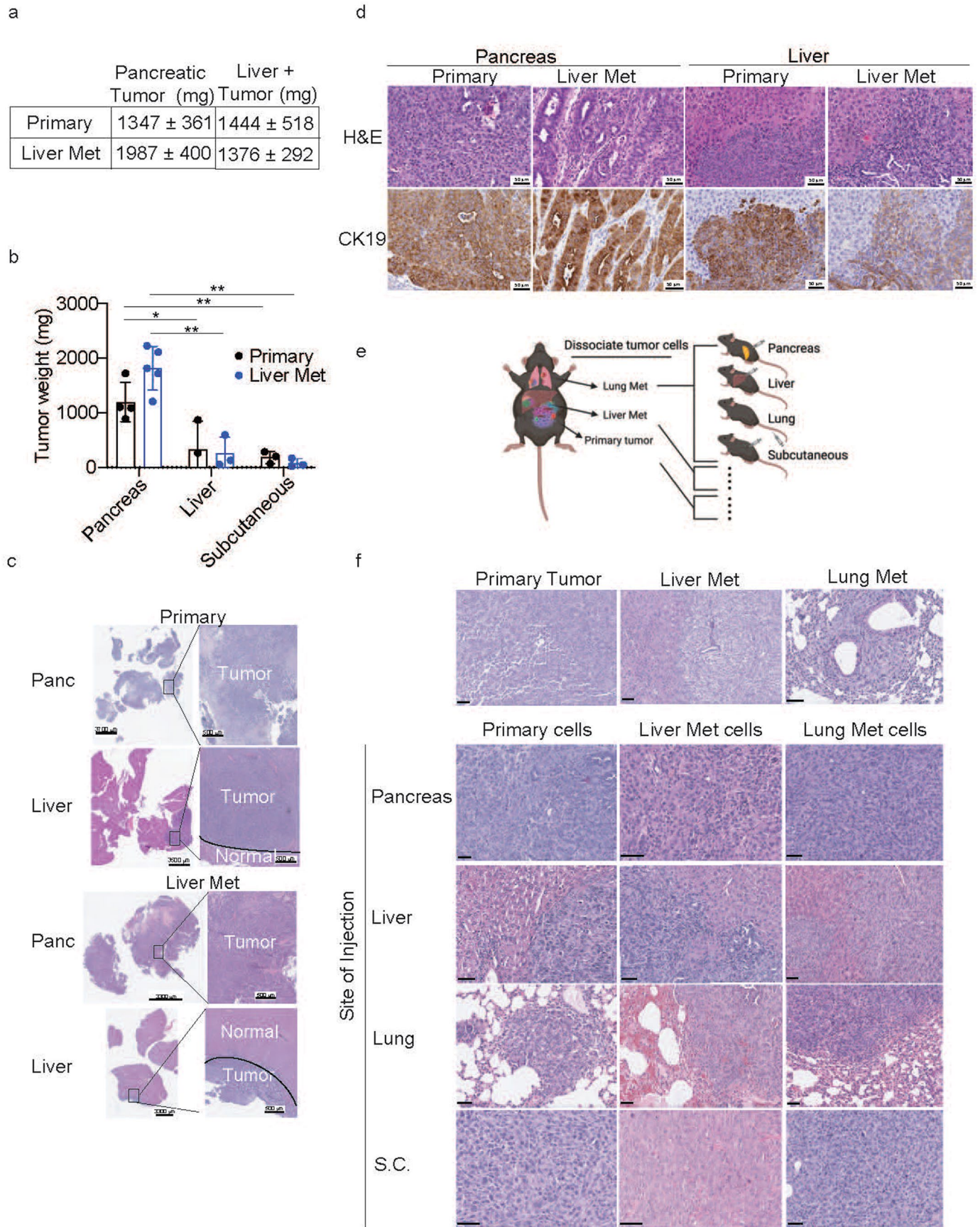
Extended Data Fig. 4 | See next page for caption.

Extended Data Fig. 4 | Characterization of pancreatic tumor transplants into the pancreas, liver, and lung. (a) Weights of pancreatic tumor tissue or liver tissue containing liver metastases (liver met) 4 weeks after implanting the same number of primary tumor- or liver metastasis-derived pancreatic cancer cells into the pancreas or the liver as indicated. Tissue weight +/− stdev; n=3-5 mice/condition. **(b)** Calculated tumor tissue weight (pancreas and liver) and tumor weight (subcutaneous) corresponding to data shown in Fig. 2b; tumor weight is calculated as the difference in tissue weight between the tumor-bearing organ and normal age-matched tissue from a non-tumor bearing mouse. For both pancreatic tumors and liver tumors, the normal tissue weight of the pancreas or the liver was subtracted to determine the calculated tumor weight, despite the observation that the entire pancreas was transformed with no macroscopic evidence of normal tissue. Subcutaneous (s.c.) tumors represent actual tumor weight. Mean+/− stdev; *p=0.045 (comparing primary cells in the pancreas vs. liver); **p=0.0011 (comparing liver met cells in the pancreas vs. liver); **p=0.0057 (comparing primary cells in the pancreas vs. the subcutaneous); **p=0.0036 (comparing liver met cells in the pancreas vs. the subcutaneous); n=3 (subcutaneous and liver), n=4 (pancreas; primary cells) n=5 (pancreas;

liver met) mice per condition. Comparisons between groups were made using a two-tailed Student's *t*-test. Multiple comparisons were done using 2way ANOVA and corrected for multiple comparisons using the Tukey test; cell line effect (p=0.3496), location effect (p < 0.0001). **(c)** Hematoxylin and Eosin (H&E) staining of tissue sections involving tumors arising from primary pancreas or liver metastatic cancer cells implanted in the pancreas or liver as indicated. The boundary between normal tissue and tumor is indicated. Scale bar- 3700 µm (lower magnification; 0.3x); 500 µm (higher magnification; 2x); Histological assessment was done for each mouse once for each independent experiment. **(d)** H&E staining and immunohistochemistry staining for CK19 in tumor tissue derived from primary or liver metastatic cancer cells that were implanted into the pancreas or the liver as indicated. scale bar, 50 µm. **(e)** Schematic depicting transplantation experiments to quantitatively assess pancreatic cancer cell proliferation in different tissue sites. Created with BioRender.com. **(f)** H&E staining of naturally arising KPC tumors (primary, liver and lung metastases (mets)) (top) or tumors resulting from transplantation of cells derived from cells isolated from the indicated primary, liver or lung metastatic tumors into each indicated site (bottom); scale bar, 50 µm.
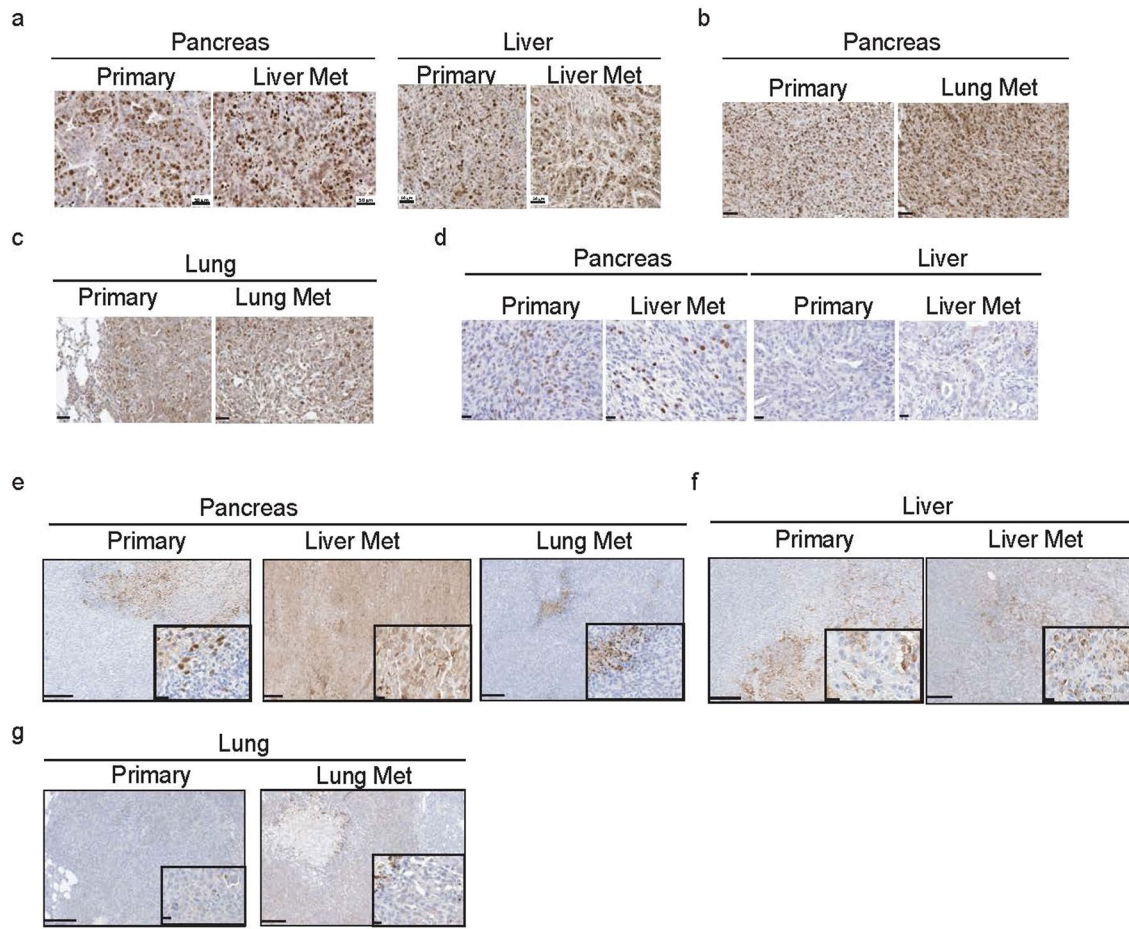
Extended Data Fig. 5 | Assessment of proliferation and cell death in tumors. (**a-c**) Ki67 staining of tumor tissue derived from primary or liver metastatic (Liver Met) pancreatic cancer cells that were implanted into the pancreas (left) or the liver (right) (a) or staining of tumor tissue from primary or lung metastatic (Lung Met) pancreatic cancer cells implanted into the pancreas (b), or lung (c) as indicated. scale bar, 50 μm. (**d**) Immunohistochemistry stain for BrdU in a representative tumor obtained from primary or liver metastatic pancreatic cancer cells injected in either the pancreas (left) or liver (right). scale bar, 20 μm. (**e-g**) Immunohistochemistry staining for cleaved caspase 3 in tumor sections derived from primary, liver, or lung metastatic pancreatic cancer cells injected in either the pancreas (e), liver (f) or lung (g). Representative region per section is shown with higher magnification image shown in the bottom right inset; scale bar for panels e-g: lower magnification- 200 μm, inset- 20 μm. For panels a-f, each image is a representative region from full scan of the entire section from 1 mouse.
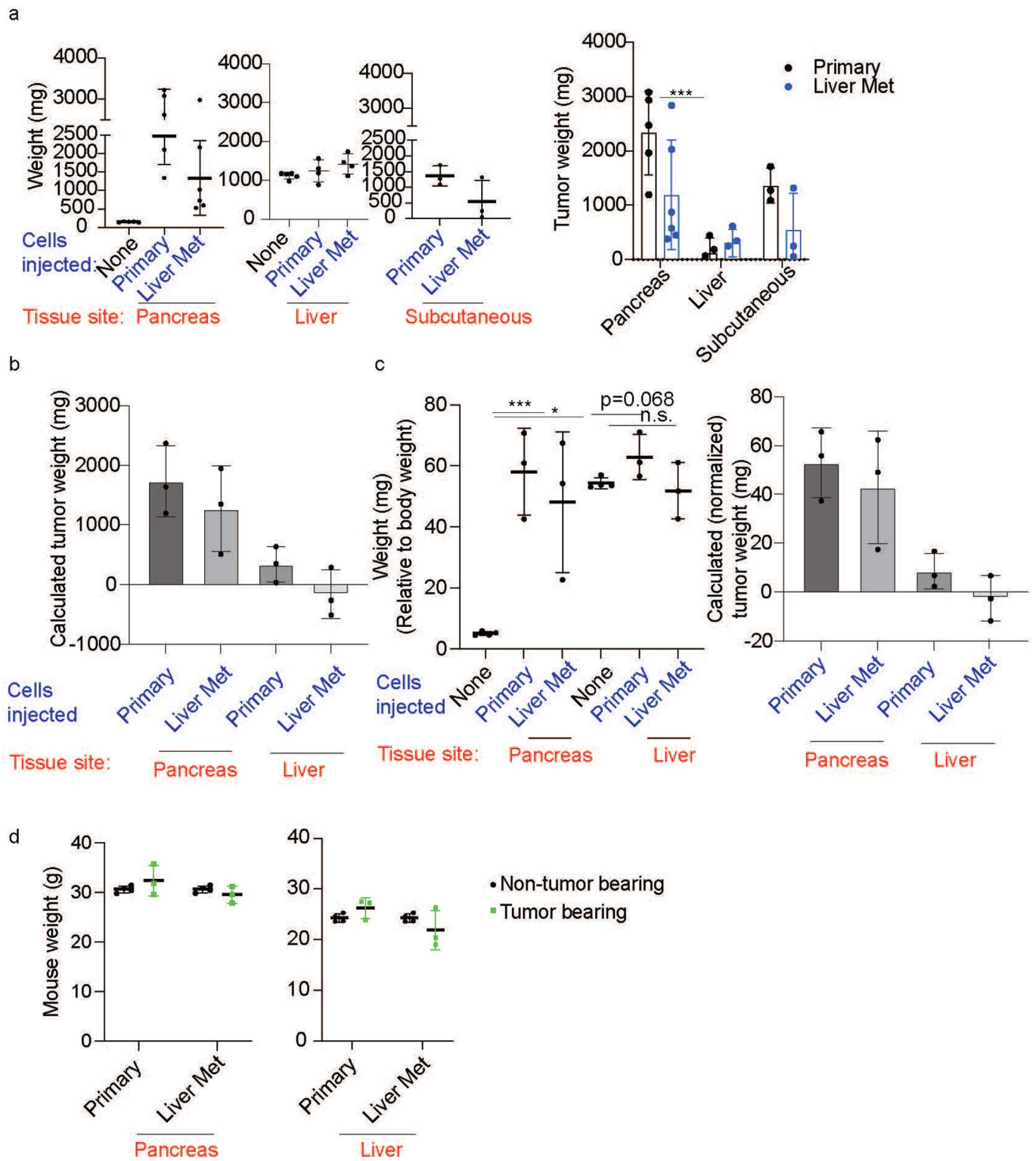
Extended Data Fig. 6 | See next page for caption.

Extended Data Fig. 6 | Independent assessment of tumor growth in pancreas and liver in immunocompetent and Nu/J mice. (**a**) Weights of the indicated tissues harvested from immunocompetent C57BL/6J mice where primary, or liver metastatic pancreatic cancer cells were implanted into the pancreas, liver, or subcutaneous space on the flank. Weight of age-matched normal pancreatic and liver tissue is also shown. n=5 (pancreas, primary and normal tissues), n=6 (pancreas, liver met); n=4 (liver), n=3 (subcutaneous) male and female mice; Mean+/− stdev; n.s.- not significant. ***p=0.0001. Also shown (right) is the calculated tumor weight (pancreas and liver) and tumor weight (subcutaneous; s.c.) for these data with tumor weight calculated as the difference in tissue weight between the tumor-bearing organ and the normal age-matched tissue from a non-tumor bearing mouse. For both pancreatic tumors and liver tumors, the normal tissue weight of the pancreas or the liver was subtracted to determine the calculated tumor weight, despite the observation that the entire pancreas was transformed with no macroscopic evidence of normal tissue. Subcutaneous (s.c.) tumors represent actual tumor weight. mean+/− stdev; ***p=0.0038. Multiple comparisons were done (right panel) using 2way ANOVA and corrected for multiple comparisons using the Tukey test; cell line effect (p=0.0520), location effect (p=0.0005). (**b**) Calculated tumor weight represented as the difference in tissue weight between tumor-bearing organ and normal age-matched tissue from non-tumor bearing age-matched immunocompromised nude (NU/J) mice; (n=3 (all samples except normal tissues (n=4)) mean+/− stdev is reported (**c**) Tissue weight from Fig. 2h, normalized to mouse body weight. (n=3 (all samples except normal tissues (n=4)) mice/group); ***p=0.0006, *p=0.0119, n.s.- not significant; mean+/− stdev (left); calculated tumor weight (as in (a)) normalized to body weight (n=3-4 mice/group); *p<0.05, n.s.- not significant; mean+/− stdev (right). Comparisons between groups were made using a two-tailed Student's *t*-test (a-c). (**d**) Weight of NU/J mice 4 weeks post-implantation of the indicated cancer cells (primary or liver met; tumor bearing mice) or sham injection (non-tumor bearing mice) into the pancreas (left) or liver (right) as indicated; n=4 (non-tumor bearing) or 3 (tumor bearing) mice/group; mean+/− stdev.

a

	Weight (mg)		
	Pancreatic Tumor	Liver + Tumor	Lung + Tumor
Primary	1376 ± 680	1408 ± 212	360 ± 180
Liver Met	1158 ± 366	1442 ± 270	n/a
Lung Met	764 ± 212	n/a	272 ± 48
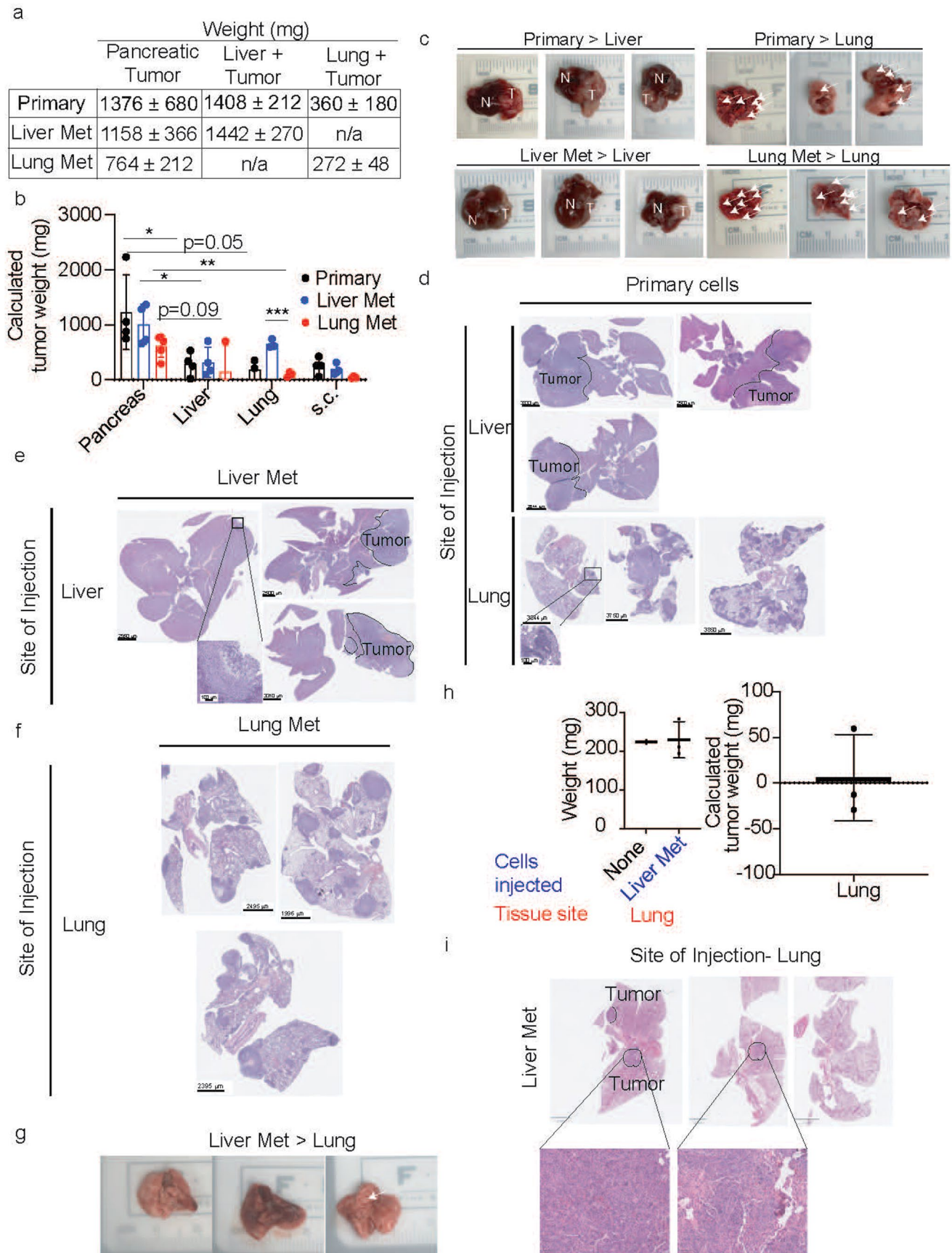
Extended Data Fig. 7 | See next page for caption.

Extended Data Fig. 7 | Characterization of pancreatic tumor transplants into the pancreas, liver, and lung. (**a**) Weights of the indicated tissues harvested from mice where primary pancreatic cancer cells, or liver or lung metastatic pancreatic cancer cells were implanted into the pancreas (pancreatic tumor), liver (liver+tumor), or lung (lung+tumor). Tissue weight +/− stdev. n=3-5 mice. (**b**) Calculated tumor weight (pancreas, liver, and lung) and tumor weight (subcutaneous) corresponding to data shown in Fig. 2k; tumor weight is calculated as the difference in tissue weight between the tumor-bearing organ and normal age-matched tissue from a non-tumor bearing mouse. For pancreatic tumors, liver tumors, and lung tumors the normal tissue weight of the pancreas, the liver, or the lung was subtracted to determine the calculated tumor weight, despite the observation that the entire pancreas was transformed with no macroscopic evidence of normal tissue. Subcutaneous tumors (s.c.) represent actual tumor weight. mean+/− stdev; *p<0.05, *p<0.01, ***p< 0.001. n=3-5 mice. Comparisons between individual groups were made using a two-tailed Student's *t*-test. Multiple comparisons were done using 2way ANOVA and corrected for multiple comparisons using the Tukey test; cell line effect (p=0.0256), location effect (p < 0.0001). (**c**) Macroscopic images of liver (left) or lung (right) four weeks post injection of cancer cells derived from a primary

pancreatic tumor (primary >) or from a liver or lung metastasis (liver met > or lung met >, respectively) into the indicated organ. N- normal tissue; T- tumor; arrows indicate tumor nodules in the lung. Each macroscopic image is from one mouse. (**d-f**) Whole mount H&E-stained liver or lung tissue from mice where primary pancreatic cancer cells (d), liver (e), or lung (f) metastatic cancer cells were implanted into the indicated site. Scale bars are indicated in the figure panels; higher magnification images are shown for smaller tumors; tumors in the liver are indicated. Histological images are shown for each individual mouse (**g**) Macroscopic images of lung four weeks post tail vein injection of pancreatic liver metastasis-derived cells. (**h**) Weights of age-matched normal lung (n=2 mice) or weights of lungs with tumors (n=3 mice) from female mice described in (g). Mean +/− stdev (left); Tumor weight is calculated as the difference in tissue weight between the tumor-bearing lung and normal age-matched lung from a non-tumor bearing mouse. Mean +/− stdev (right). (**i**) Whole mount H&E-stained lung tissue from mice injected with pancreatic liver metastases via tail vein. Scale bar- 2 mm. Higher magnification is shown on the bottom; scale bar- 100 μM. Histological image is from each mouse and is an independently repeated experiment from an independently derived cell line to accompany data shown in Fig. 2k and Extended Data Fig. 7b.
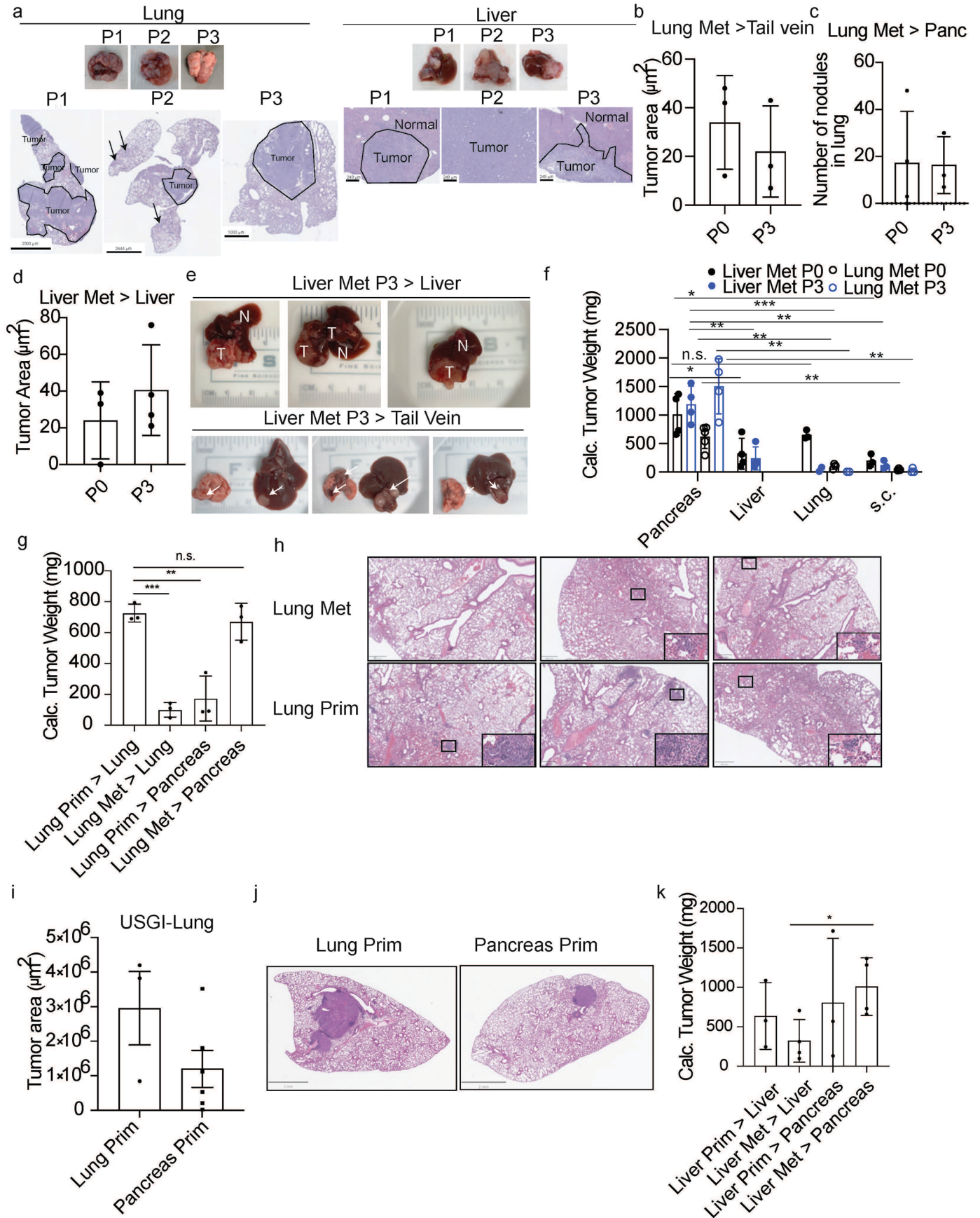
Extended Data Fig. 8 | See next page for caption.

Extended Data Fig. 8 | Passaging pancreatic tumors in the lung or liver of mice selects for increased seeding of the metastatic tissue and analysis of primary liver and primary lung cancer cells. (**a**) Macroscopic tissue images and histology assessing that tissue after each passage where cells from a lung metastasis (top) or liver metastasis (bottom) were serially implanted to from tumors in each organ. P1-P3 refers to each passage. Tumor areas indicated by boundary or arrows. (**b**) Quantification of lung metastases generated when parental (P0) or P3 lung metastatic pancreatic cancer cells were injected into the tail vein of wild type mice (left). Tumor area was calculated as the area of the tumor divided by the total area of tissue for all lung sections as assessed by H&E staining. Mean +/− stdev; n=3 mice/condition. (**c**) Quantification of the number of lung nodules generated when parental (P0) or P3 lung metastatic pancreatic cancer cells were implanted to form a tumor in the pancreas (right). Mean +/− stdev; n=3 (all conditions except P0 (n=4)) mice/condition. (**d**) Quantification of liver metastases generated when parental (P0) or P3 liver metastatic pancreatic cancer cells were injected into the liver. Tumor area was calculated as the area of the tumor divided by the total area of tissue for all liver sections as assessed by H&E staining; Mean +/− stdev; n=3 (P0) and n=4 (P3) mice. (**e**) Macroscopic images of liver (top) or lung and liver (bottom) after implantation of P3 liver metastatic pancreatic cancer cells (Liver Met P3 >) into the Liver (top) or the tail vein (bottom) as indicated. N- normal tissue; T- tumor; arrows indicate tumor nodules in the lung or liver. (**f**) Calculated tumor tissue weight (pancreas, liver, and lung) and tumor weight (subcutaneous) corresponding to data shown in Fig. 3b–e; tumor weight is calculated as the difference in tissue weight between the tumor-bearing organ and normal age-matched tissue from a non-tumor bearing mouse. Subcutaneous tumors represent actual tumor weight. For pancreatic tumors, liver tumors, and lung tumors the normal tissue weight of the pancreas, the liver, or the lung was subtracted to determine the calculated

tumor weight, despite the observation that the entire pancreas was transformed with no macroscopic evidence of normal tissue. Mean+/− stdev; n=4 (pancreas; all cells except Lung Met P0 (n=5)), n=4 (liver), n=3 (lung, all cells except Liver Met P3 (n=4), n=3 (subcutaneous) mice/condition *p<0.05, **p<0.01, ***p<0.001; n.s.- not significant. Comparisons between groups were made using a two-tailed Student's t-test (**g**) Calculated tumor weight corresponding to relevant data shown in Fig. 3b–d and Fig. 4a. Tumor weight is calculated as the difference in tissue weight between the tumor-bearing organ and normal age-matched tissue from a non-tumor bearing mouse. For pancreatic tumors, liver tumors, and lung tumors the normal tissue weight of the pancreas, the liver, or the lung was subtracted to determine the calculated tumor weight. Mean+/− stdev; n=3 mice/condition *p<0.05, **p<0.01, ***p<0.001; n.s.- not significant. Comparisons between groups were made using a two-tailed Student's t-test. (**h**) Histology of tumor sections corresponding to intratracheal injection of indicated cancer cells into the lung that relate to data shown in Fig. 4b. (**i**) Ultrasound guided injection (USGI) of primary lung cancer cells or pancreatic cancer lung metastases into the lung and quantification of tumor area. Each data point represents one mouse and n=3 (lung primary cells) and n=6 (pancreas primary cells) mice; mean +/− stdev (**j**) Representative histology of tumor sections that related to data shown in (c) showing single tumor nodule formation in the lung following UGSI. Scale bar is 2 mm. (**k**) Calculated tumor weight corresponding to data shown in Fig. 4c as well as data in Fig. 3b–d. Tumor weight is calculated as the difference in tissue weight between the tumor-bearing organ and normal age-matched tissue from a non-tumor bearing mouse. For pancreatic tumors and liver tumors the normal tissue weight of the pancreas and the liver was subtracted to determine the calculated tumor weight. Mean+/− stdev; n=3 (liver primary, pancreas and liver) and n=4 (liver metastases, pancreas and liver) mice/condition *p<0.05. Comparisons between groups were made using a two-tailed Student's t-test.

a

Lung adenocarcinoma

Lung

Liver

b

HCC

Lung

Liver

c

d

Lung Media
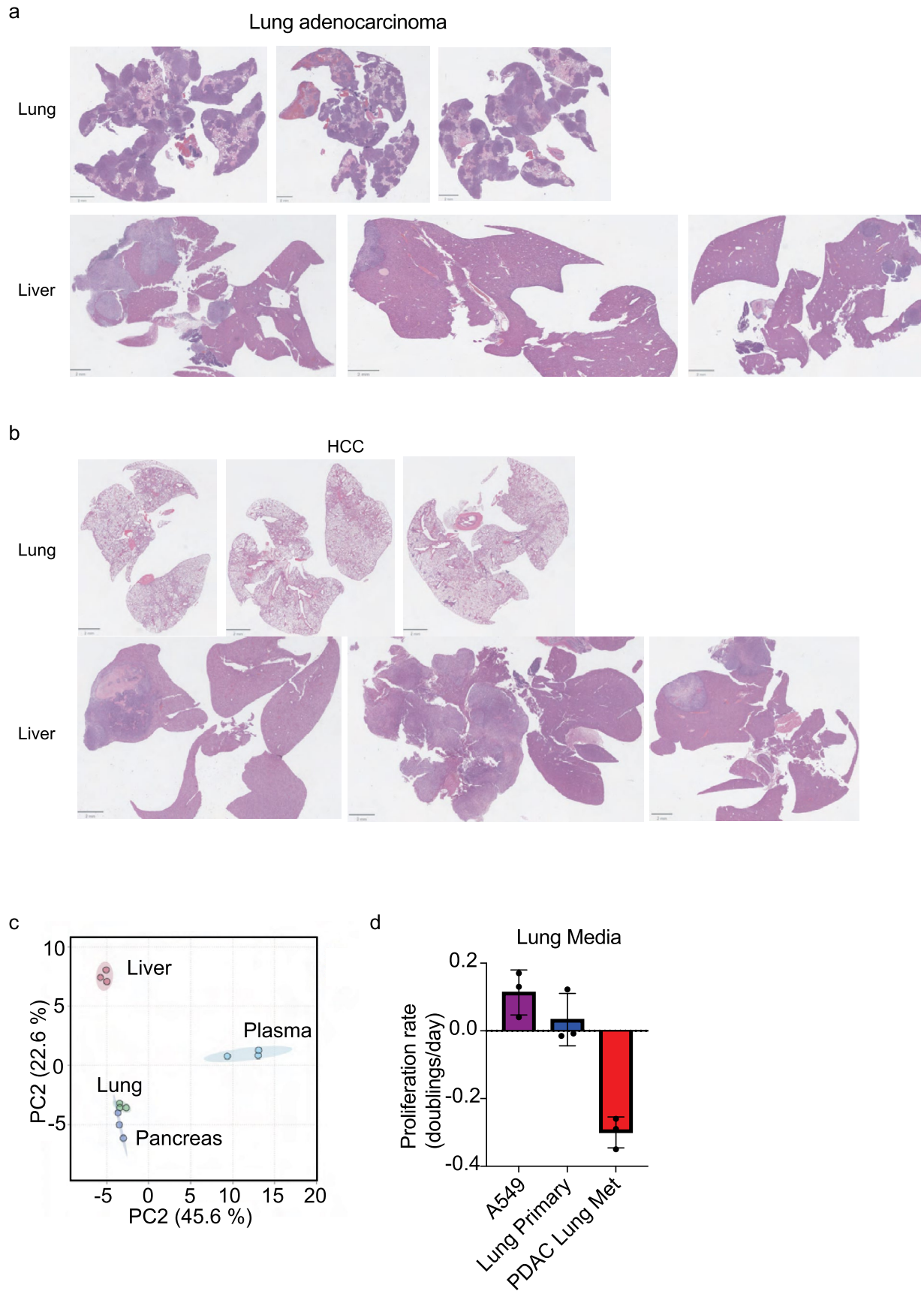
Extended Data Fig. 9 | See next page for caption.

Extended Data Fig. 9 | Histology images of primary lung and primary liver tumors and assessment of metabolite levels in tissues. (**a-b**) H&E stained histology sections of tumors obtained from injection of primary lung cancer cells into either the lung (top) or liver (bottom) (a) or from injection of primary liver cancer cells (HCC) into the lung (top) or liver (bottom) (b). n=3 mice/condition; data accompany tumor area data shown in Fig. 4d, e. (**c**) Principal component analysis (PCA) plot showing the separation of metabolite levels measured in pooled in interstitial fluid form indicated organs or plasma from wild-type non-tumor bearing animals. (**d**) Proliferation rate of primary lung cancer cells (human A549 cells or mouse KP primary lung cancer cells) and cells from a KPC pancreatic cancer lung metastasis (lung met) in media formulated to mimic metabolite levels measured in lung interstitial fluid (lung media); average of n=3 biological replicates were used for A549 cells and pancreatic lung met cells and average of n=2 biological replicates were used for the lung primary cells; mean +/− stdev.
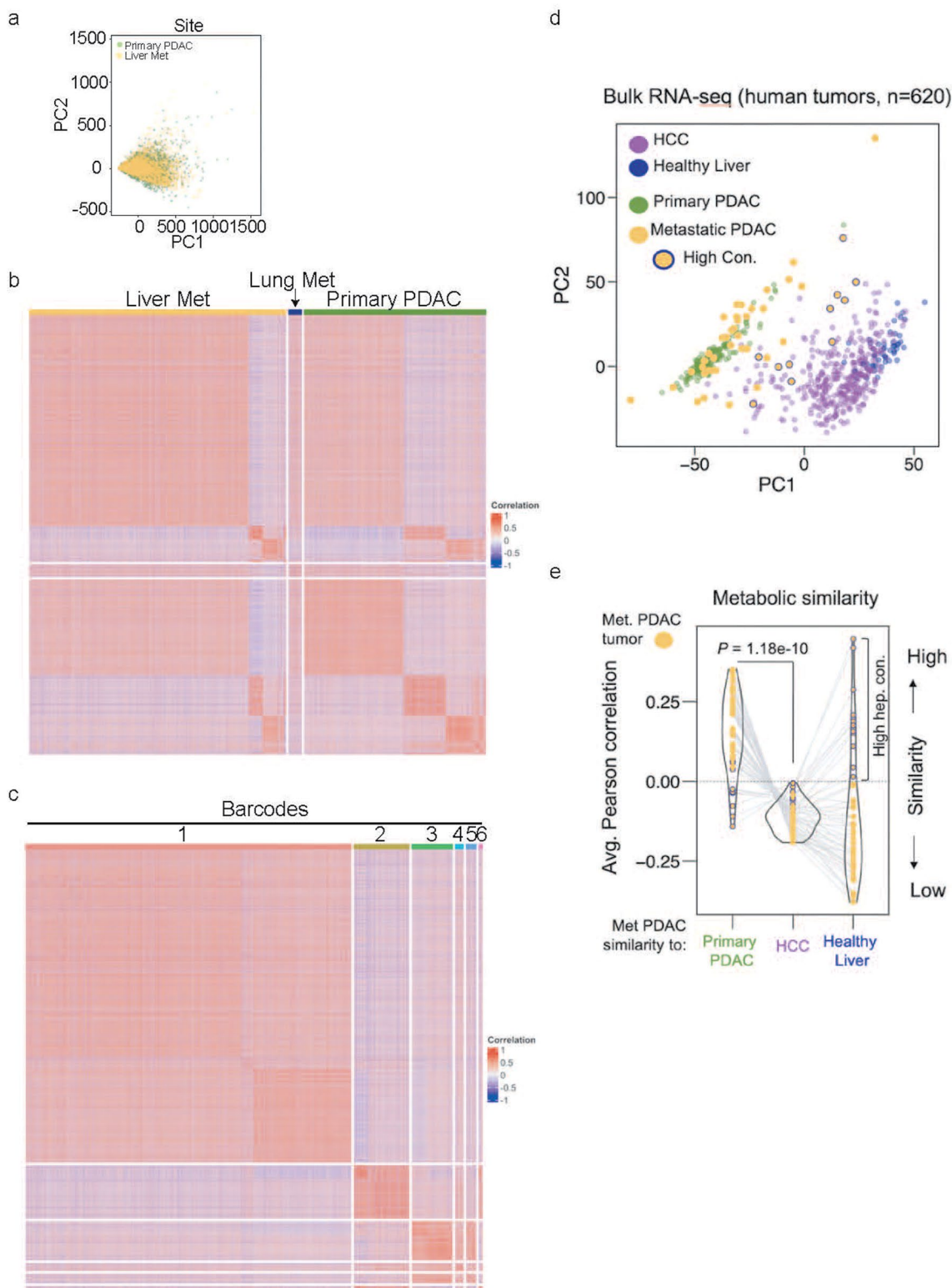
Extended Data Fig. 10 | Analysis of metabolic gene expression from mouse and human tissues. (a-c) Metabolic gene expression derived from scRNA-seq data[27] that is another representation of the data presented in Fig. 4g, h. Data represented as entire cell populations and comparing primary pancreatic cancer (PDAC) and liver metastases (liver met) arising in the mouse KPC PDAC model (a); A cross correlation of metabolic gene expression between pairs of single cells are plotted ordered by either site (b), or barcode (c); within a given barcode, pairs of cells tend to have high correlations in their metabolic expression, whereas there are subsets of cells within sites that have different metabolic gene expression but these subsets of cells do not separate based on tissue site; that is a given barcode across has similar metabolic gene expression across metastatic sites. **(d)** PCA of a human RNA-seq dataset[39,40] comparing metabolic gene expression in primary pancreatic tumors (Primary PDAC; green), liver metastatic PDAC (yellow), hepatocellular carcinoma (HCC; purple), and healthy liver (blue) as indicated. **(e)** Average Pearson correlation comparing metabolic similarity between pancreatic liver metastases (Met PDAC; yellow data points) to primary tumors (Primary PDAC), hepatocellular carcinoma (HCC) or healthy liver. Liver metastatic PDAC with higher Pearson correlation to HCC and healthy liver contains a higher degree of hepatocyte contamination (circled yellow data points) in (d) and (e). The p-value was determined using paired two-tailed Student t-test comparing Primary PDAC to HCC for the Met PDAC tumors.

nature portfolio

Corresponding author(s):   Matthew G. Vander Heiden

Last updated by author(s):   Jun 14, 2024

Reporting Summary

Nature Portfolio wishes to improve the reproducibility of the work that we publish. This form provides structure for consistency and transparency in reporting. For further information on Nature Portfolio policies, see our Editorial Policies and the Editorial Policy Checklist.

Statistics

For all statistical analyses, confirm that the following items are present in the figure legend, table legend, main text, or Methods section.

n/a	Confirmed	
☐	☒	The exact sample size (*n*) for each experimental group/condition, given as a discrete number and unit of measurement
☐	☒	A statement on whether measurements were taken from distinct samples or whether the same sample was measured repeatedly
☐	☒	The statistical test(s) used AND whether they are one- or two-sided *Only common tests should be described solely by name; describe more complex techniques in the Methods section.*
☐	☒	A description of all covariates tested
☐	☒	A description of any assumptions or corrections, such as tests of normality and adjustment for multiple comparisons
☐	☒	A full description of the statistical parameters including central tendency (e.g. means) or other basic estimates (e.g. regression coefficient) AND variation (e.g. standard deviation) or associated estimates of uncertainty (e.g. confidence intervals)
☐	☒	For null hypothesis testing, the test statistic (e.g. *F*, *t*, *r*) with confidence intervals, effect sizes, degrees of freedom and *P* value noted *Give P values as exact values whenever suitable.*
☒	☐	For Bayesian analysis, information on the choice of priors and Markov chain Monte Carlo settings
☒	☐	For hierarchical and complex designs, identification of the appropriate level for tests and full reporting of outcomes
☒	☐	Estimates of effect sizes (e.g. Cohen's *d*, Pearson's *r*), indicating how they were calculated

Our web collection on statistics for biologists contains articles on many of the points above.

Software and code

Policy information about availability of computer code

Data collection	No software was used for data collection
Data analysis	Mass spectrometry data was analyzed using El-Maven software (version 0.9.1) from Elucidata. Natural abundance correction for mass isotopologue distributions was corrected using IsoCorrectoR. Graphs and associated statistics were all generated using GraphPad Prism software (version 9.4.1). Tumor initiating capacity was calculated using ELDA software. LCMS data was analyzed using Compound Discoverer 3.1 (Thermo Scientific).

For manuscripts utilizing custom algorithms or software that are central to the research but not yet described in published literature, software must be made available to editors and reviewers. We strongly encourage code deposition in a community repository (e.g. GitHub). See the Nature Portfolio guidelines for submitting code & software for further information.

Data

Policy information about availability of data

All manuscripts must include a data availability statement. This statement should provide the following information, where applicable:
- Accession codes, unique identifiers, or web links for publicly available datasets
- A description of any restrictions on data availability
- For clinical datasets or third party data, please ensure that the statement adheres to our policy

Any associated Extended Data Figures, Extended Data Tables, and Nature Portfolio reporting summary are provided.

Research involving human participants, their data, or biological material

Policy information about studies with [human participants or human data](). See also policy information about [sex, gender (identity/presentation), and sexual orientation]() and [race, ethnicity and racism]().

Reporting on sex and gender	n/a
Reporting on race, ethnicity, or other socially relevant groupings	n/a
Population characteristics	n/a
Recruitment	n/a
Ethics oversight	n/a

Note that full information on the approval of the study protocol must also be provided in the manuscript.

Field-specific reporting

Please select the one below that is the best fit for your research. If you are not sure, read the appropriate sections before making your selection.

☒ Life sciences ☐ Behavioural & social sciences ☐ Ecological, evolutionary & environmental sciences

For a reference copy of the document with all sections, see [nature.com/documents/nr-reporting-summary-flat.pdf]()

Life sciences study design

All studies must disclose on these points even when the disclosure is negative.

Sample size	Power calculations for animal studies was performed using G*Power 3.1 software. Based on the power analysis, an effect size of 9.835 (alpha=0.05, power=0.80) would be achieved with n=2 mice/group for the cells injected into the pancreas. For the liver transplants, an effect size of 3.452 (alpha=0.05, power=0.80) could be achieved with n=3 mice/group. For the lung transplants (via tail vein), an effect size of 5.1583 (alpha=0.05, power=0.80) could be achieved with n=3 mice/group. Finally for the subcutaneous transplants, an effect size of 3.957 (alpha=0.05, power=0.80) could be achieved with n=3 mice/group. Based on these calculations, at least 3 mice were included in each experimental condition at the beginning of the experiment.
Data exclusions	No data was excluded from analysis.
Replication	All key experiments were repeated in both males and females where possible. For metabolomics experiments, normal tissue from 3 males and 3 females were collected at the same time of the day. For LCMS analysis on tumors and liver metastases, 3 male mice and 1 female mouse was included.
Randomization	All surgical procedures were done in a random (but not blinded) manner to account for cell viability and other factors. All animal studies ere age-matched within 1-2 weeks of each other.
Blinding	Animal experiments were not blinded.

Reporting for specific materials, systems and methods

We require information from authors about some types of materials, experimental systems and methods used in many studies. Here, indicate whether each material, system or method listed is relevant to your study. If you are not sure if a list item applies to your research, read the appropriate section before selecting a response.

Materials & experimental systems

n/a	Involved in the study
☐	☒ Antibodies
☐	☒ Eukaryotic cell lines
☒	☐ Palaeontology and archaeology
☐	☒ Animals and other organisms
☒	☐ Clinical data
☒	☐ Dual use research of concern
☒	☐ Plants

Methods

n/a	Involved in the study
☒	☐ ChIP-seq
☐	☒ Flow cytometry
☒	☐ MRI-based neuroimaging

Antibodies

Antibodies used	mCherry (1:500 dilution; Novus Biologicals: NBP1-96752), GFP (1:250 dilution; Novus Biologicals: NB600-308), pan-cytokeratin (1:500 dilution; Abcam: ab133496), Ki67 (1:250 dilution; Novus Biologicals: NB110-89717), BrdU (1:2000 dilution; Abcam: ab6326), or Cleaved Caspase 3 (Asp 175) (1:400 dilution; Cell Signaling 9661); G12D mutant Kras (Cell Signaling 14429)
Validation	Validation performed for Kras G12D using cells that express WT Kras or Kras G12C mutation

Eukaryotic cell lines

Policy information about cell lines and Sex and Gender in Research

Cell line source(s)	All mouse cells were generated from KPC (C57BL/6J LSL-Kras(G12D);Trp53fl/fl;Pdx1-Cre) or KPCT (C57BL/6J LSL-Kras(G12D);Trp53fl/fl;Pdx1-Cre; TdTomato) PDAC model. Mouse liver cancer cell line was established from hepatic tumors as published. Lung adenocarcinoma cells were obtained from lung cancer model (LSL-Kras(G12D); Trp53fl/fl; Ad-Cre) as published.
Authentication	All cell lines generated were validated using mutant Kras specific antibody, by sequencing the cell line, or in addition to western blotting by presence of recombined Kras allele by genotyping.
Mycoplasma contamination	Cells were tested for mycoplasma at the time of generation and every 10 passages using MycoAlert Plus Kit (Lonza). Cells were not maintained in culture for more than 20 passages or replaced roughly every 2-3 months.
Commonly misidentified lines (See ICLAC register)	n/a

Animals and other research organisms

Policy information about studies involving animals; ARRIVE guidelines recommended for reporting animal research, and Sex and Gender in Research

Laboratory animals	C57BL/6 mice (both males and females) were used. For transplantation experiments, mice between 8-10 weeks were used in the study. Nu/J mice (both males and females) roughly 8-10 weeks of age were used for transplantation experiments in immunocompromised mice.
Wild animals	n/a
Reporting on sex	Both males and females were used for all studies. For transplantation experiments, for primary cell line 1: male mice were used; liver met cell line: male mice were used; lung met: male mice (tail vein, intrahepatic), males and females (pancreas), females (subcutaneous); For primary cell line 2: male mice were used; For primary cell line 3: male mice were used. For in vivo adapted cell lines- liver adapted: female mice (tail vein, liver, subcutaneous, and orthotopic); lung adapted: males and females (tail vein), female mice (liver, subcutaneous), male and female (pancreas). For limiting dilution analysis: male mice were used. For metabolomics experiments: normal tissues were derived from males and females; for tumor bearing animals- 3 males and 1 female was used. For immunocompromised mice experiments Nu/J mice from Jackson labs (both males and females) were used.
Field-collected samples	n/a
Ethics oversight	All experiments were done in accordance with the MIT Committee on Animal Care.

Note that full information on the approval of the study protocol must also be provided in the manuscript.

Plants

Seed stocks	n/a
Novel plant genotypes	n/a
Authentication	n/a

Flow Cytometry

Plots

Confirm that:

☒ The axis labels state the marker and fluorochrome used (e.g. CD4-FITC).

☒ The axis scales are clearly visible. Include numbers along axes only for bottom left plot of group (a 'group' is an analysis of identical markers).

☒ All plots are contour plots with outliers or pseudocolor plots.

☒ A numerical value for number of cells or percentage (with statistics) is provided.

Methodology

Sample preparation	Tumors were dissected, minced, and digested at 37⬚C for 30 min with 1 mg/mL Collagenase I (Worthington Biochemical, LS004194), 3 mg/mL Dispase II (Roche, 04942078001), and 0.1 mg/mL DNase I (Sigma, D4527) in 5 mL PBS. After 30 min, cells were incubated with EDTA to 10 mM at room temperature for 5 min. Cells were filtered through a 70 mm cell strainer, washed twice in PBS, and cells resuspended in flow cytometry staining buffer (Thermo Fischer, 00-4222-57) for fluorescent protein expression analysis on a BD-LSR II flow cytometer.
Instrument	BD-LSR II flow cytometer
Software	Analysis was done using FlowJo software Version 10
Cell population abundance	Whole tumors were digested as described in sample preparation and at least 10,000 cells (or 50,000 cells) for the liver samples were analyzed.
Gating strategy	Unlabeled cells were included in each run. For the competition experiments with tumor samples, unlabeled cancer cell lines were included as a control. Gating strategy is provided in supplemental figure 2.

☒ Tick this box to confirm that a figure exemplifying the gating strategy is provided in the Supplementary Information.